U.S. DEPARTMENT OF THE INTERIOR

U.S. GEOLOGICAL SURVEY

MARINE GEOLOGIC INVESTIGATIONS OF DISENCHANTMENT BAY, ALASKA, AFTER BREAKUP OF 1986 HUBBARD GLACIER ICE DAM

RV KARLUK CRUISE K1-91-YB
21-28 JUNE 1991

by

Paul R. Carlson[1]
Ross D. Powell[2]
Ellen A. Cowan[3]
Daniel E. Lawson[4]

Open-File Report 92-706

1992

1. U.S. Geological Survey, Menlo Park, CA 94025
2. Geology Dept. Northern Illinois U., Dekalb, IL 60115
3. Dept. of Geology, Appalachian St. U., DeKalb, IL 60115
4. USA, CRREL, Hanover, NH 03755

We entered the ice-infested waters of Disenchantment Bay on the 42 foot research vessel, the *KARLUK* precisely one hundred and one years after I.C. Russell visited Disenchantment Bay by canoe. He described the scene as follows--"the island (Haenke) occupies the position of the stage in a vast amphitheatre; the spectators are hoary mountain peaks, each a monarch robed in ermine and bidding defiance to the ceaseless war of the elements. How insignificant the wanderer who confronts such an audience, and how weak his efforts to describe such a scene!"

INTRODUCTION

Cruise K1-91-YB to Disenchantment Bay, which forms the upper part of Yakutat Bay, Alaska (Fig. 1), was designed to study the glacimarine sedimentary environment associated with the magnificent Hubbard Glacier, at the northern boundary of Disenchantment Bay. This study is a continuation of previous studies of morainal bank and proximal environments of tidewater glaciers in Glacier Bay, Alaska (Powell, 1991a; Cowan and Powell, 1991; Carlson et al, 1983). These earlier studies relied upon sediment sampling and high-resolution seismic-reflection profiling to delineate sedimentary facies in tidewater glacier environments. The most recent work (Powell, 1991b; Powell et al., 1991) has made use of an additional powerful tool, a submersible Remotely Operated Vehicle (ROV) to make visual observations of the glacier's tidewater face, grounding line morainal banks, and the associated fjord floor. On cruise K1-91-YB we faced more severe ice and current conditions than we had encountered in Glacier Bay. In spite of these formidable obstacles, we were able to collect about 140 km of high-resolution seismic-reflection and 7 kHz bathymetric trackline profiles (Fig. 2). We also made six successful dives with the ROV system, on which, in addition to obtaining video footage, data were gathered by the attached conductivity, temperature, depth (CTD), optical backscatter (OBS), and current meters. In addition, water column vertical profiles were obtained using the ROV sensors at three sites. In this report, we will briefly discuss the data collected by the various systems deployed.

EQUIPMENT SYSTEMS

1. REMOTELY OPERATED VEHICLE.

The submersible ROV is a Phantom DHD2 with a 500m data transmission cable. The ROV has a CoHo low-light black and white video camera and two- 250 watt tungsten-halogen lights as basic equipment. The system was deployed with optional equipment that included a Sanyo CCTV color video camera, a Nikonis stereo still camera with strobe, an EDO side-scan sonar fish, a Marsh-McBirney electromagnetic current meter, a Downing and Assoc. optical backscatterance (OBS) turbidity monitor, and a Seacat SBE 19 CTD system.

2. HIGH-RESOLUTION SEISMIC-REFLECTION PROFILING

The Geopulse subbottom profiling system was operated at a power setting of 350 J and a firing rate of one-half second. The high-resolution seismic-

reflection profiles were collected using a Benthos 15/30 hydrophone, filtered between 300 and 1000 Hertz, on a EPC 4800 recorder at a one-half second sweep rate.

3. BATHYMETRY.

A 7 kHz Raytheon RTT 1000 hull-mounted transducer/transceiver was utilized to collect bathymetric and high-resolution profiles.

4. WATER-COLUMN SAMPLING

A 2.5 liter van Dorn water bottle was used to obtain water samples at various depths throughout the water column to measure concentrations of suspended matter at different locations in the fjord. Each sample was collected by hand lowering the bottle on separate casts.

5. NAVIGATION

Navigation throughout Disenchantment Bay was controlled by radar and Magellan GPS 2000 unit. Radar was the primary navigation system because the high, steep fjord walls prevented consistent GPS readings.

PHYSICAL SETTING

GEOGRAPHY

Disenchantment Bay occupies the northern part of Yakutat Bay, one of the prominent glacially formed bays adjacent to the north-eastern part of the Gulf of Alaska (Fig. 1). Yakutat Bay, a triangular shaped feature, is about 60 km long (from the Gulf of Alaska to Hubbard Glacier) and nearly 30 km wide at the seaward end (Fig. 1). The most northerly part of the bay, the more elongate Disenchantment Bay (Figs. 1 & 3), is about 15 km long and 5 km wide with high steep bedrock walls that consist primarily of slightly metamorphosed Cretaceous sedimentary rocks of the Yakutat Group (Plafker and Miller, 1958). The 100 m-high, 7 km wide ice cliff of Hubbard Glacier, the widest tidewater terminus in North America, forms the northern end of Disenchantment Bay. Three smaller glaciers, Miller, Haenke, and Turner, calve into Disenchantment Bay from the northwest. Prominent along the eastern side of the bay is the 1.5 X 1 km Haenke Island which has a maximum elevation of about 170 m. Further north-northeast, small unnamed islands and rocks protrude above the bay water, some emergent only at low tide. The steep east wall of the bay continues north to nearly 60° N Latitude where Gilbert Point forms the north end of a massive peninsula that separates Russell Fjord from Yakutat Bay. The opening into Russell Fjord is presently narrower and shallower because of the recent advance of Hubbard Glacier.

GLACIAL HISTORY

Yakutat Bay owes much of its configuration to glaciation that has been modifying this fjord basin throughout most of Neogene and Quaternary time. As recently as 600-900 years ago (Plafker and Miller, 1958), the ancestral Hubbard Glacier occupied the bay, extending slightly beyond the mouth into the Gulf of Alaska as indicated by a large arcuate terminal morainal bank that encompasses the bay entrance (Fig. 1). Two other possible morainal banks have been identified in Yakutat Bay. The "mid-bay moraine"? (Wright, 1972) may extend about two thirds of the way across the bay and the "upper-bay moraine", first identified by Gilbert (1904), extends easterly across the bay from Blizhni Point (Fig. 1). Plafker and Miller (1958) have suggested that this "upper-bay moraine" was formed during a more recent advance of the Hubbard Glacier ~200 years ago.

The ponded basins between the morainal banks contain thicknesses of glacimarine sediment up to 350 m, which suggests maximum sedimentation rates that range from 20 to 70 cm/a (Carlson, 1989). The sediment on the morainal banks is a diamicton and in the basins ranges from clayey silt containing iceberg-rafted pebbles to silty clay (Wright, 1972; Carlson et al., 1978).

Although most of Yakutat Bay has been ice-free and receiving glacimarine suspended sediment for more than 200 years, Disenchantment Bay has experienced periodic advances of the Hubbard Glacier terminus. Russell (1891) and Gilbert (1904) have suggested that visits to Yakutat Bay by Malaspina in 1792 and Vancouver in 1794 chronicled the presence of Hubbard Glacier south of Haenke Island. Tarr and Martin (1914) report that Russian maps showed the terminus to be a short distance north of Haenke Island in the early 1800s and also showed a lake to be present in Russell Fjord, indicating damming of the fjord entrance by Hubbard Glacier. By the time of the Harriman expedition's visit to Disenchantment Bay in 1899, the Hubbard Glacier had retreated about 3.5 km north of Osier Island (Gilbert, 1904, plate VIII). Tarr and Martin (1914) showed maps of the terminus of Hubbard Glacier that in 1909 was about 1.9 km from Osier Island and 1910 was yet another 0.32 km distant.

For the next 60 years, the glacier slowly advanced, causing Post and Mayo (1971) to predict that "around 1990" Russell Fjord would again be dammed by the advancing terminus. On May 29, 1986, an ice dam blocked the entrance to Russell Fjord and Russell Lake filled with fresh water eventually to a height of 25.5 m (Mayo, 1989). On October 8, 1986, the ice dam failed catastrophically, producing a peak discharge of 105,000

m^3 s^{-1} averaged over one hour (Mayo, 1989). Although the outbreak occurred at night and could not be observed until about 5 hours later, the turbid outburst plume at that time had a measured surface speed at the center of the flow of 11.0 m s^{-1} which provided enough momentum for the highly turbulent flow to reach the face of Turner Glacier about 6 km across Disenchantment Bay (Mayo, 1989). Seitz et al., (1986) reported that the turbid jokulhlaups plume was later visible at the mouth of Yakutat Bay, a distance of more than 50 km from the ruptured dam. Mayo (1989) also reported that 50 m of erosion of the highly jointed rocks of Osier Island and 200-300 m of an alluvial outwash fan attached to Gilbert Point were removed by the jokulhlaups. Trabant et al., (1991) predict that Russell Fjord at the present rate of glacial advance, will be closed off again during this decade. The rapid advance is due to a high accumulation-area to total-glacier-area ratio (0.95), and the presence of a morainal bank that controls ice loss from calving. They suggest that this time the dam might be sufficient to cause the lake to build to a height of 40 m, and to flow out of the south end into the Situk River drainage.

OCEANOGRAPHY

There are few oceanographic observations available for the Yakutat Bay area. The oceanography of Russell Fjord was reported by Reeburgh et al., (1976). As part of their study, temperature and salinity data were collected on April 5, 1973 from one station in upper Yakutat Bay located 10 km downfjord from Haenke Island. Their measurements at 50 m depth are lower in temperature (by 1.6° C) and higher in salinity (by 1.1‰) than those collected during our cruise in late June 1991. This difference can be explained by the location of their station which was closer to the mouth of the bay, by tidal cycle variations related to the "flushing" of Russell Fjord, and by annual variations in temperature and salinity in the Gulf of Alaska (Royer, 1975), the source water for Yakutat Bay. The depth of the outermost sill which controls exchange between the Bay and the Gulf of Alaska is at 70 m (Reeburgh et al., 1976). In April 1973, Reeburgh et al., (1976) measured surface water that was warmer (by 1.08° C) and higher in salinity (by 6.68 ‰) than our measurements showed in June 1991. This difference results from the seasonal increase in meltwater discharge and by the closer proximity of our stations to the face of Hubbard Glacier.

PRELIMINARY RESULTS

CRUISE COMMENTS

The initial cruise plan was to concentrate on ROV dives in Disenchantment Bay intended to study the submerged face of Hubbard Glacier and the underlying morainal banks. Because of the great quantity

of ice that was constantly calving the accessible areas were limited. It soon became evident that the predesigned plan would be modified by the daily ice and current patterns. As a result of the severe ice and current conditions, our bathymetric and seismic-reflection survey lines were very disrupted (Fig. 2a&b) and there were parts of the Disenchantment Bay that never were reached during the cruise.

BATHYMETRY

The hull-mounted 7 kHz system was utilized continually on all profile lines and provided bathymetric data for the areas traversed. Prior to this cruise, the most complete and recent bathymetric data for Disenchantment Bay had been collected by the National Oceanic and Atmospheric Agency (NOAA) in 1978. The NOAA smooth sheet data, from Hydrographic Surveys 9778 and 9779 were contoured to provide detailed work sheets for our cruise K1-91-YB (Fig. 3).

Bathymetric data were collected previously from a helicopter along the face of the Hubbard Glacier where the risk to a small vessel would be very high due to the calving of ice from the 100-m-high ice cliff (Trabant et al., 1991). Water depths at the terminus ranged from as deep as 104 m along the northwestern 1/3 of the ice cliff to as shallow as 77 m along the southeastern 1/3 of the Hubbard Glacier ice face. The water shoals to 8 m at the entrace to Russell Fjord and depth increases near the ice face in Russell Fjord to as deep as 81 m.

Comparison between our data and the NOAA bathymetric data indicates shoaling has occurred throughout the deep basin (Fig. 4). The shoaling typically ranges from 2 to 6 m, with a maximum of 11 m at the base of the slope WNW of Osier Island. Although there is a general across- and down-fjord trend, two large distinct areas of sediment accumulation can be identified. An area of maximum shoaling occurs within the upper part of the deep fjord basin, west and northwest of Osier Island. The amount of accumulation generally decreases west and southwest across the basin toward the Turner Glacier terminus. The second area of accumulation occurs within the deep basin west of Haenke Island where up to 5 m of shoaling has occurred (Fig. 4). In addition, localized areas of greater shoaling are apparent, occurring at the base of the fjord slope below Turner Glacier, and the southern most mapped area of the Bay.

We attribute much of the shoaling to sediment eroded and transported by the outburst flood of Russell Lake on October 8, 1986, (Seitz et. al., 1986; Mayo, 1989). The up-Bay area of maximum shoaling and the across-and down-fjord decrease lie along the path of the outburst flood as

described by Mayo, (1989) and Seitz et al., (1986) (Figs. 3&4). Following ice dam failure, the outburst flood rushed from between Osier Island and Gilbert Point, at speeds reaching 11 m S^{-1}. The outburst flood continued across Disenchantment Bay as a highly turbulent "stream" that impinged upon the terminus of Turner Glacier (Mayo, 1989). Here the flow was deflected in a general down-fjord direction, west of Haenke Island (Fig. 3). Discharge velocity would have decreased with emergence into Disenchantment Bay and flow into and across the deep basin, which concurs with the across fjord thickness decrease. Eddies resulting from the outburst "stream" would have established gyres north and south of the flow where reduced velocity and turbulence would have favored sedimentation from the overflow plume (Figs. 3&4).

Because of the impressive scouring action of the jokulhlaups, a large amount of sediment was eroded and transported. In the Gilbert Point area, shore erosion of 50 to 300 m and up to 50 m of bedrock were eroded by the outburst flood (Mayo, 1989). Bedrock 2-3 m deep on Osier Island and a 200 to 300 m long alluvial fan deposit off Gilbert Point were eroded by the flood waters and transported into the upper bay area. In addition, over 500 m of glacier retreat near the outburst point resulted (Mayo, 1989), widening the channel, and likely eroding morainal bank material in the process. The upper-bay area of sediment accumulation lies immediately down-flow from both erosional areas.

The area of 11 m shoaling lies downslope of the Hubbard Glacier's 1986 terminus position which resulted from a rapid ice advance that shoved and transported significant volumes of marine sediment (Fig. 3). Mayo (1989) reported that a >600 m length of the ice margin near the entrance to Russell Fjord developed an emergent push moraine during this advance. Outburst flood induced erosion resulting in failure of this push moraine could account for some of this 11 m thick sequence.

The basin fill west of Haenke Island likewise lies along the path of the outburst flood waters during the period of maximum discharge following its deflection off the Turner Glacier terminus and the western fjord wall (Figs. 3&4). Subsequently, as discharge gradually decreased over the next 10 to 15 hours, the flow path would have returned to more central areas of the Bay. The deep waters south of the Turner Glacier terminus as well as reduced velocities resulting from decreased discharge would favor deposition.

Subaqueous slope failures and sediment flows along the western basin slope are also a possible consequence of the outburst flood. Such

flows would tend to follow the general gradient of the basin slope and floor into the basin west of Haenke Island. As described in the following section, seismic profiles in this basin have revealed both bed and sub-surface features which appear to be sediment flow toes (Fig. 4). However, these deposits may have been generated by subaqueous flows during, or subsequent to the outburst flood, and derived from any number of locations within the Bay. Additional investigations, including coring, will be required to fully interpret the shoaling and seismic data collected during this cruise.

SUBBOTTOM PROFILES

This section describes some of the features visible on the high-resolution seismic-reflection profiles collected in various parts of Disenchantment Bay (Fig. 2a) and the six lines obtained in the upper part of Yakutat Bay (Fig. 2b). Features resolved on the profiles include bedrock underlying the fjord sediment basin, sediment thickness, reflections within the sediment pile, the morainal bank on which the front of Hubbard Glacier rests, the "upper-bay moraine", and features such as mass movement deposits within the profiles.

The sedimentary fill accumulating in the bedrock basin of Disenchantment Bay reaches thicknesses of more than 150 m. The upper part of the sediment column is characterized by flat-lying continuous reflections, some of which can be traced across the width of the basin (Fig. 5). Note the bedrock walls delineating the sides of the sedimentary basin. At the base of the fjord walls, most of the high-resolution profiles show hummocky disrupted reflections that indicate slide or debris flow deposits (Figs. 5&6). Other mass movement deposits can be seen at depth in the sediment. Two lines from the west side of upper Yakutat Bay (Figs. 7&8) exhibit well-defined mass movement scars with the resulting debris visible on the fjord floor at the base of the wall. Note that above the scar on Figure 8 there are a series of small step scarps that indicate the prevalence of mass movement. In this area, slides and debris flows are probably related to the rapid accumulation of sediment on the delta that forms Blihzni Point. These and other mass movements could have been triggered by seismic loading generated by the numerous earthquakes that occur in this tectonically active region. Along the west wall of the fjord south of Turner Glacier, two adjacent crossings show an irregular, hummocky buried deposit that may be a submarine slide or debris flow deposit (Fig. 9).

Profiles collected as close as feasible to the 100 m high ice face of Hubbard Glacier show the character of the distal slope of the morainal bank to be an irregular, hummocky surface with no visible internal reflections, the product of mass movement from this "pinning point" moraine (Fig. 10 a&b). The gradient of this part of the morainal bank averages about 3° and attains a maximum steepness of about 4° along the profiled section of the bank. This contrasts to a gradient of about 14° for the proximal slope calculated from the near glacier end of our profile (183 m depth) to the nearest shallowest water depth at the glacier face (81 m) as measured from a helicopter by Trabant et al., (1991).

South of the lower end of Disenchantment Bay lie prominent ridges that form the "upper-bay moraine", (Fig. 11). The most southern ridge is the steepest, having a gradient of 14.5° on the upper part of the morainal bank (similar in value to the Hubbard Glacier morainal bank), decreasing to 9.5° on the lower third of the bank, and then to 1° over some hummocky terrain that appears to be mass movement debris. If we calculate the gradient of slope across the lower third of the morainal bank, and the slide or debris flow deposit, we obtain a value of 2.6°, a gradient close to that measured for the distal part of the Hubbard morainal bank. Thus, we might conjecture that the "upper-bay moraine" is a possible morphologic model for the present morainal bank of Hubbard Glacier. Note the ponded glacimarine mud, containing iceberg-rafted pebbles (Carlson et al., 1978) in basins between minor morainal banks that are progressively smaller in the up-bay direction, presumably formed successively by the glacier during retreat.

One question we posed before the cruise was whether or not we could find any remnant depositional features on the fjord floor that may have been caused by the outburst flood (jokulhlaup) when the ice dam at Russell Fjord failed. Several of the high-resolution seismic-reflection profiles that crossed the fjord floor west and southwest of Haenke Island showed a very subtle bump or scarp-like feature having a relief of about 2 m (Fig. 12). On Figure 4, west-southwest of Haenke Island, we have plotted the occurrences of the shallow scarps that we thought possibly might represent the toes of debris or mud flows that could have been generated by the jokulhlaup. However, their plotted configuration does not necessarily point to the Russell Fjord entrance area as the origin of all of these features. The presence of the three glaciers along the west wall of the fjord and, of course, the mighty Hubbard Glacier at the head of the bay, all provide sources of rapidly deposited sediment that could fail and flow or slide down into the fjord.

A high-resolution acoustic profile near Haenke Island, contains a buried lens-shaped feature (Fig. 13) that also might be a debris flow deposit--again a number of potential sources are nearby. This wedge or lens is buried beneath 2-3 m of the most recent sediment. If as reported in several fjords, including Yakutat Bay (Carlson, 1989), the rate of sediment accumulation is >100 cm/a and in extreme cases several times that rate (Molnia et al., 1984; Cowan et al., 1988; Powell, 1991a), then the upper 2-3 m thick layer could have been deposited since 1986. Consequently, the lens could have been part of the slug of sediment discharged into Disenchantment Bay when the jokulhlaupss from Russell Fjord occurred on October 8, 1986.

WATER COLUMN AND BOTTOM SEDIMENT DATA FROM ROV DIVES

Real-time CTD and OBS data and video imagery, were collected and transmitted through the ROV's umbilical to the ship during each of the six dives (Fig. 14). Temperature, salinity, sigma-t, and OBS turbidity measurements were plotted against depth for each ROV descent through the water column. Current velocity and direction also were measured; however, many of these values are unuseable due to current and ice-induced movement resulting in ROV instability. The descent rate was uniform, therefore, these profiles are similar to oceanographic casts. However, most of the profiles were collected from ice-proximal locations that were targeted for visual observation rather than evenly spaced stations for oceanographic study. Water samples were collected at various depths at sites 2, 3, 5 and 6, (Fig. 14) with a 2.5 L van Dorn bottle.

At dive site 1, located near the lower end of Disenchantment Bay (Fig. 14), the water column had a salinity minimum from 8.9 to 11 m depth that resulted from an interflow (Fig. 15). The sigma-t value within this layer was 0.72 units less than the overlying water column above 8.9 m. There was also an abrupt increase in OBS turbidity units at 9.9 m that remained high until a depth of 15.6 m. A suspended sediment concentration of 7.2 g/L would be necessary to offset this low sigma-t layer at this depth. No water samples were collected during this dive, therefore, no suspended sediment concentrations are reported. However, concentrations as high as 7 g/L are within the range of suspended concentrations measured from an interflow in a fjord in Glacier Bay (Cowan et al., 1988). The fact that OBS turbidity values remained at a moderate level until 50 m depth indicates that sedimentation from the interflow was quite rapid. Current speeds were measured at depths at 19, 62, 76, and 86 m. Corresponding speeds were 60, 81, 80, and 61 cm/s.

The profile at dive site 2 (same location as site 1; Fig. 14) indicates a 26 m thick overflow (Fig. 16a). The overflow had the lowest salinity and temperature and the highest OBS turbidity readings measured on this dive. The highest sediment concentrations (Table 1) are within the overflow, but they remain high down to 60 m depth where there is a gradual decrease in turbidity to about 90 m depth. Video observations show that the base of the higher turbidity zone is marked by large, "wispy" billows of mud and marine snow (phytoplankton and some zooplankton). Beneath the 26 m thick surface layer, the temperature gradually increases to a maximum of about 6.8° C between depths of 80 and 105 m. Salinity similarly increases below 26 m depth. Salinity gradually increases, temperature decreases, and OBS fluctuates at low values (mostly due to marine snow) below 100 m depth. This profile is similar to those described from other glacial fjords in British Columbia and Alaska (Cowan and Powell, 1990; Pickard, 1961, 1967). The distinct halocline indicates that the freshwater supply, mainly from glaciers at the head of the Bay and from Russell Fjord, is sufficient to drive circulation in the upper part of the water column. The high suspended sediment concentrations are also associated with the overflow indicating that it originates from meltwater discharge. Current velocities could only be measured at 216 m depth (74 cm/s), and at the bed (101 cm/s). The video imagery of the bed at this site shows a relatively flat, featureless, soft, sandy mud.

Dive site 3 (Fig. 14) is similar in water column profile to site 2, but more proximal to Hubbard Glacier. The overflow is thinner, about 17 m thick, but has OBS turbidity values three times higher than at site 2 (compare - Fig. 16 a&b). Dive site 3 is closer to Hubbard Glacier, an important freshwater and sediment source, than site 2. The water column below the halocline is similar to that at site 2 (Figs. 16 a&b). Current speeds at the seabed were low (26 cm/s). Water column video observations suggest that current flow was mainly vertical; the horizontal component averaged 20 cm/s. Problems with ice, wind, and tidal currents affecting the *Karluk's* station keeping, caused this dive to be aborted before ice face and morainal bank observations could be made.

The profile for dive site 4 (Fig. 14) was collected over the slope adjacent to the entrance to Russell Fjord. During the descent the tide was ebbing and surface currents were flowing out of Russell Fjord past the dive site. The more uniform temperature on descent than measured at the other sites indicated a well-mixed water column. Salinity gradually increases throughout the profile (Fig. 17a). Turbidity is highest in the overflow, reaching peaks at about 4 m and 15 m depth. Within the overflow, sediment concentrations fluctuated in response to ebb-induced

turbulence that was seen on the video as billowing turbid clouds. An ascent profile (Fig. 17b) was collected 20 minutes later, after the tide had turned to flood and surface water began to move from the Bay into Russell Fjord. The effects of this reversal included an increase in salinity above 52 m and a decrease in OBS turbidity beneath the overflow plume, (compare Figs. 17 a&b). Temperatures remained relatively uniform and similar to the descent profile. The video showed that at dive site 4 the bed at 62 m depth consists primarily of "soupy" mud with slightly irregular relief. Iceberg-rafted clasts up to cobble size are scattered across the bed. Video of the bed showed a strong current with large flocs and marine snow in turbulent transport flowing down Disenchantment Bay away from the entrance of Russell Fjord. Initially the current exhibited episodic turbulent pulses ranging in speed from 40 to 50 cm/s, but after about 15 minutes the turbulent flow decreased to a non-turbulent, uniform flow of about 26 cm/s, still moving out of Russell Fjord during the initial tidal flooding stage.

Dive site 5 (Fig. 14) was occupied for visual observations of the suspended particulate matter (SPM) in the water column. As is common in glacial fjords, the turbidity maximum in the overflow occurs below the surface (Fig. 18), coinciding with the lowest temperature in the overflow (Cowan and Powell, 1990). The base of the overflow, about 20 m depth, is marked by a sharp halocline and thermocline and a decrease in SPM concentration, below which, a few flocs occur with marine snow. Below 110 m, flocs are few and OBS turbidity values are low and variable. A slight increase in the number of flocs occurs at about 170 m depth, coinciding with a weak, lower temperature, nepheloid layer. The fjord floor at 220 m depth consists of soft, "soupy" mud with cm-scale relief. The video shows ripples that are cut by a small scarp 1-4 cm high trending perpendicular to ripple crests that strike at about 243° MN. Isolated cobble- to small boulder-size iceberg-rafted clasts are scattered over the fjord floor. Shrimp were common and four bottom fish were imaged. Near-bottom currents in the nepheloid layer were flowing at 21 cm/s between 207 and 297° MN. At 207 m depth, a current speed of 22 cm/s was measured. At 120 m depth, turbulent bursts up to 80 cm/s punctuated quieter flow conditions of 23 cm/s.

The profiles at dive site 6, (Fig. 14) were also collected in a more distal location for determining water column characteristics (Figs. 19 a&b). This dive was about two hours later than the dive at site 5. Characteristics of the upper part of the water column in the overflow were similar in both profiles; however, the rest of the column was different. At dive site 6, there were four significant increases in OBS

turbidity values that correlated with video observations of increased numbers of flocs in the water column (Fig. 19a). The layer between 20 and 30 m was probably produced by particles settling from the base of the overflow. Between 40 and 60 m, an OBS turbidity peak was associated with a lower density layer or interflow. The upper part of the interflow is characterized by the highest current velocities (Fig. 19b). Current velocities ranging from 18 to 65 cm/s were measured during ascent at dive site 6 (Fig. 19b). At 40 m depth, currents were strong enough to cause the ROV to spin continuously. The current speeds are relatively uniform throughout the water column except for the higher velocity layer between 40 and 60 m.

The difference in sigma-t values between the layer at 40-60 m and the overlying denser layer is small (0.2315 units), but it represents an unstable density profile if only the water density is considered. However, this difference could be offset by the addition of suspended sediment in a concentration of approximately 2.3 g/L. Water samples collected from this station had suspended sediment concentrations of less than 100 mg/L, but none were collected within the 40-60 m depth layer. At about 50-55 m depth the temperature, salinity, and OBS values show relatively abrupt changes. Note that the OBS turbidity values do not drop sharply at the base of the layer as do the salinity values, indicating that particles were settling out from the interflow at 40-60 m depth.

Below the interflow, the water column was dominated by marine snow but there were also two well defined layers of flocs. These layers were observed on video and also identified by peaks in OBS turbidity values between 85 and 97 m, and between 155 and 160 m depth. Each of these layers occurs just above a small density contrast on the sigma-t profile (Fig. 19a).

Below about 225 m depth the numbers of flocs increased to the bottom, reflected by increasing OBS values. This increase defines a 9 m-thick nepheloid layer of colder, more saline water. The top of the nepheloid layer appeared "billowy" on the video. At about 1-2 m above the fjord bottom the water column was quite turbid. The bed is very "soupy" mud. The bottom current was flowing at about 24 cm/s in a down-fjord direction.

CONCLUSIONS

1. Comparing K1-91 bathymetic profiles to NOAA 1978 bathymetry shows shoaling of the deep fjord floor by 2-6 meters. An exception is at the base

of the slope west of the Russell Fjord entrance area where 8-11 meters of shoaling has occurred. This decrease in water depth ostensibly is due to the breakup of the Hubbard Glacier ice dam in October 1986, resulting in large scale erosion, sediment transport into Disenchantment Bay, and redeposition.

2. High-resolution seismic-reflection profiles across the deep floor of Disenchantment Bay WSW of Haenke Island show subtle, low-relief seafloor scarps that may be the toes of flows generated by the jokulhlaup of October 8, 1986. Some of these flows also may have come from moraines of the Hubbard Glacier or the side-wall glaciers.

3. High-resolution seismic-reflection profiles indicate that more than 150 m of sediment has accumulated in Disenchantment Bay basin since deglaciation. This sedimentation is a result of a combination of processes that include slide and gravity flow deposition that originates from the steep fjord side walls and from the morainal banks that are terminal moraines of Hubbard Glacier. Other important processes include particulate settling from the meltwater discharge plumes issuing from Hubbard and the smaller side-wall glaciers of Disenchantment Bay and Russell Fjord and iceberg rafting of sediment.

4. The present gradient of the Hubbard Glacier morainal bank decreases down fjord from ~14^0 to 3^0. The "upper-bay moraine", located in the upper part of Yakutat Bay, has similar gradients--14.5^0 at the top part and averaging 2.6^0 over the lower part of the moraine. This similarity in morphology suggests that the "upper-bay moraine" is a satisfactory model for the modern morainal bank.

5. The tidewater glacier meltwater discharge and tidal currents dominate the water column properties of Disenchantment Bay. Interflows, possibly from high suspended matter discharge from Hubbard Glacier and perhaps the ebb-flow from Russell Fjord, create small density inversions in the water column. ROV dives and water samples also recorded the presence of a 26 m thick overflow near Hubbard Glacier. Suspended sediment concentrations were highest at the dive site closest to Hubbard Glacier (Table 1). Concentrations reached 602 mg/L in the overflow. On the slope west of the Russell Fjord entrance, ROV imagery showed strong, turbulent, down-fjord transport of large flocs and marine snow at 5-7 m above the bottom. In the deep water of the fjord axis west of Haenke Island, a 9-m-thick nepheloid layer was defined by the ROV data.

ACKNOWLEDGMENTS

We greatly appreciate the professional skippering of Jim Christmann, Santa Cruz, CA as a last-minute, skillful, substitute captain. Mike Boyle enthusiastically provided much needed electonics expertise and willing assistance in all phases of the cruise. We thank Sue Hunt and Judi Allen for their thorough logistical help, and we appreciate the assistance given to us by members of the U.S. National Forest Service in Yakutat. A sincere thank you goes to Gayle Ranney of Fishing and Flying in Yakutat for providing great help with communications, transportation, and logistical advice. Water depths were picked from the 7kHz bathymetric profiles by Christen Nall, a student at Appalachian State University. Funding for the cruise was provided by National Science Foundation Grant DPP 8822098 to R. Powell, by CRREL for D. Lawson's participation, and by the U.S. Geological Survey. Reviews by Dennis Trabant and Homa Lee were very helpful. We appreciate the assistance of Carolyn Degnan and Jean Riordan in plotting and merging the shoreline and tracklines and preparing the bathymetric and trackline maps used in the field and in the open-file report.

REFERENCES

Atwood, T.A., Bruns. T.R., Carlson, P.R., Molnia, B.F., and Plafker, G., 1981. Bathymetric map of the eastern Gulf of Alaska. Scale, 1:250,000. U.S. Geological Survey Miscellaneous Field Study Map MF-859, 3 sheets.

Carlson, P.R., 1989. Seismic reflection characteristics of glacial and glacimarine sediment in the Gulf of Alaska and adjacent fjords. Marine Geology, v. 85, p. 391-416.

Carlson, P.R., Molnia, B.F., Hampson, J.C., Jr., Post, A., and Atwood, T.J., 1978, Post-deglaciation sedimentation in Yakutat Bay, Alaska. Transactions, American Geophysical Union, EOS, v. 59, p. 296.

Carlson, P.R., Wheeler, M.C., Molnia, B.F., Post, A., and Powell, R.D., 1983, Map showing post-neoglacial thickness and bathymetry *in* Tarr Inlet, Glacier Bay, Alaska. U.S. Geological Survey Miscellaneous Field Studies Map, MF-1456.

Cowan, E.A., and Powell, R.D., 1990. Suspended sediment transport and deposition of cyclically interlaminated sediment in a temperate glacial fjord, Alaska, U.S.A. In Glacimarine Environments: Processes and Sediments, Dowdeswell, J.A. and Scourse, J.D. (eds). Geological Society of London Special Publication 53, p. 75-89.

Cowan, E.A., and Powell, R.D., 1991. Ice-proximal sediment accumulation rates in a temperate glacial fjord, southeast Alaska. *In* Anderson, J.B. and Ashley, G.M. (eds.), Glacial Marine Sedimentation -- Paleoclimatic Significance. Geological Society of America Special Paper 261, p. 75-93.

Cowan, E.A., Powell, R.D., and Smith, N.D., 1988. Rainstorm induced event sedimentation at the tidewater front of a temperate glacier. Geology, v. 16, p. 409-412.

Gilbert, G.K., 1904. Glaciers and glaciation: Harriman Alaska Expedition, v. 3, New York, Doubleday, Page & Co.

Mayo, L.R., 1989, Advance of Hubbard Glacier and 1986 outburst of Russell Fiord, Alaska, U.S.A. Annals of Glaciology, v. 13, p. 189-194.

Molnia, B.F., Atwood, T.J., Carlson, P.R., Post, A., and Vath, S.C., 1984. Map of marine geology of upper Muir and Wachusett inlets, Glacier Bay, Alaska: sediment distribution and thickness, bathymetry and interpreted seismic profiles. U.S. Geological Survey, Open-file Report 84-632, scale 1:40,000.

Plafker, G. and Miller, D.J., 1958. Glacial features and surficial deposits of the Malaspina District, Alaska. U.S. Geological Survey Miscellaneous Geologic Investigations Map I-271.

Pickard, G.L., 1961. Oceanographic features of inlets in the British Columbia mainland coast. Journal of the Fisheries Research Board of Canada, 18, p. 907-999.

Pickard, G.L., 1967. Some oceanographic characteristics of the larger inlets of southeast Alaska. Journal of the Fisheries Research Board of Canada, 24, p. 1475-1506.

Post, A., and Mayo, L.R., 1971. Glacier-dammed lakes and outburst floods in Alaska. U.S. Geological Survey Hydrologic Atlas HA-455, 10 p., 3 pl.

Powell, R.D., 1991a Grounding-line systems as second order controls on fluctuations of temperate tidewater termini. *In* Anderson, J.B. and Ashley, G.M., (eds). Glacial Marine Sedimentation -- Paleoclimatic Significance. Geological Society of America Special Paper 261, p. 75-93.

Powell, R.D., 1991b Grounding-line systems as feedbacks for marine glacier stability: further evaluations from ROV submersible observations. 13th INQUA Congress, Beijing, China, Abstracts Volume: p. 287.

Powell, R.D., Lawson, D.E., Cowan, E.A., Hunter, L.E., Cai, J., and Carlson, P.R., 1991, Submersible observations of grounding lines and morainal banks of tidewater termini of temperate glaciers. Annual Geological Association of Canada Program with Abstracts, p. 101.

Reeburgh, W.S., Muench, R.D., and Cooney, R.T., 1976. Oceanographic conditions during 1973 in Russell Fjord, Alaska. Estuarine and Coastal Marine Sciences, 4, p. 129-145.

Royer, T.C., 1975. Seasonal variations of waters in the northern Gulf of Alaska. Deep-Sea Research, 22, p. 403-416.

Russell, I.C., 1891. An expedition to Mount St. Elias. National Geographic Magazine, v. 3, p. 53-191.

Seitz, W.G., Thomas, D.S., and Tomlinson, B., 1986. The storage and release of water from a large glacier-dammed lake: Russell Lake near Yakutat, Alaska. U.S. Geological Survey Open-File Report 86-545, 9p.

Tarr, R.S., and Martin, L., 1914. Alaskan glacier studies. National Geographic Society, Washington, D.C., 498 p.

Trabant, D.C., Krimmel, R. M., and Post, A. 1991. A preliminary forecast of the advance of Hubbard Glacier and its influence on Russell Fjord, Alaska. U.S. Geological Survey Water Resources Investigations Report 90-4172, 34p.

Wright, F.F., 1972. Marine Geology of Yakutat Bay, Alaska. U.S. Geological Survey Professional Paper 800-B, p. B9-B15.

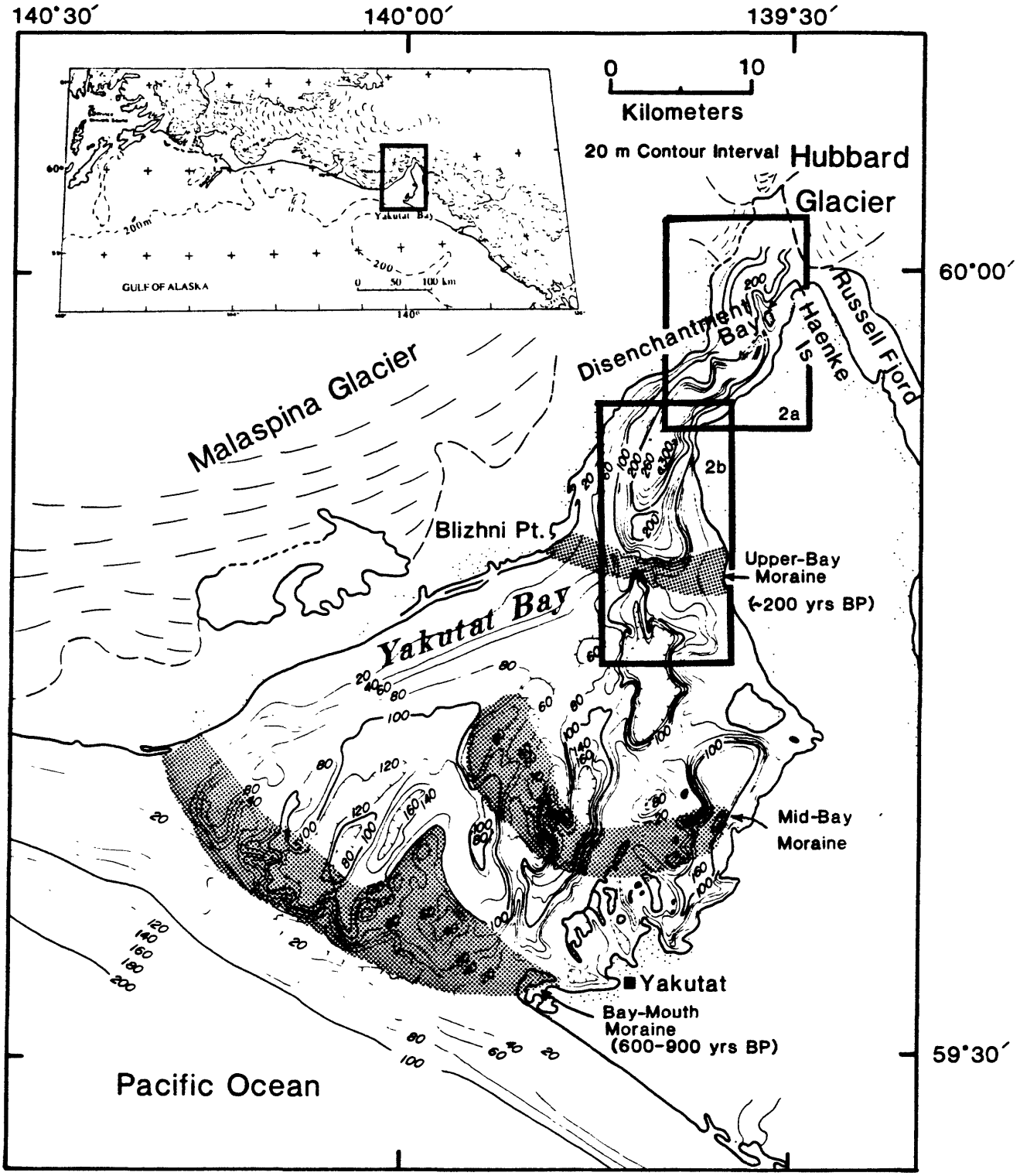

Figure 1. Map showing location of Yakutat Bay, Disenchantment Bay, and Hubbard Glacier along northern Gulf of Alaska coast line. Detailed bathymetry is from Atwood et al., 1981. Areas of figures 2a and b are delineated by bold rectangles.

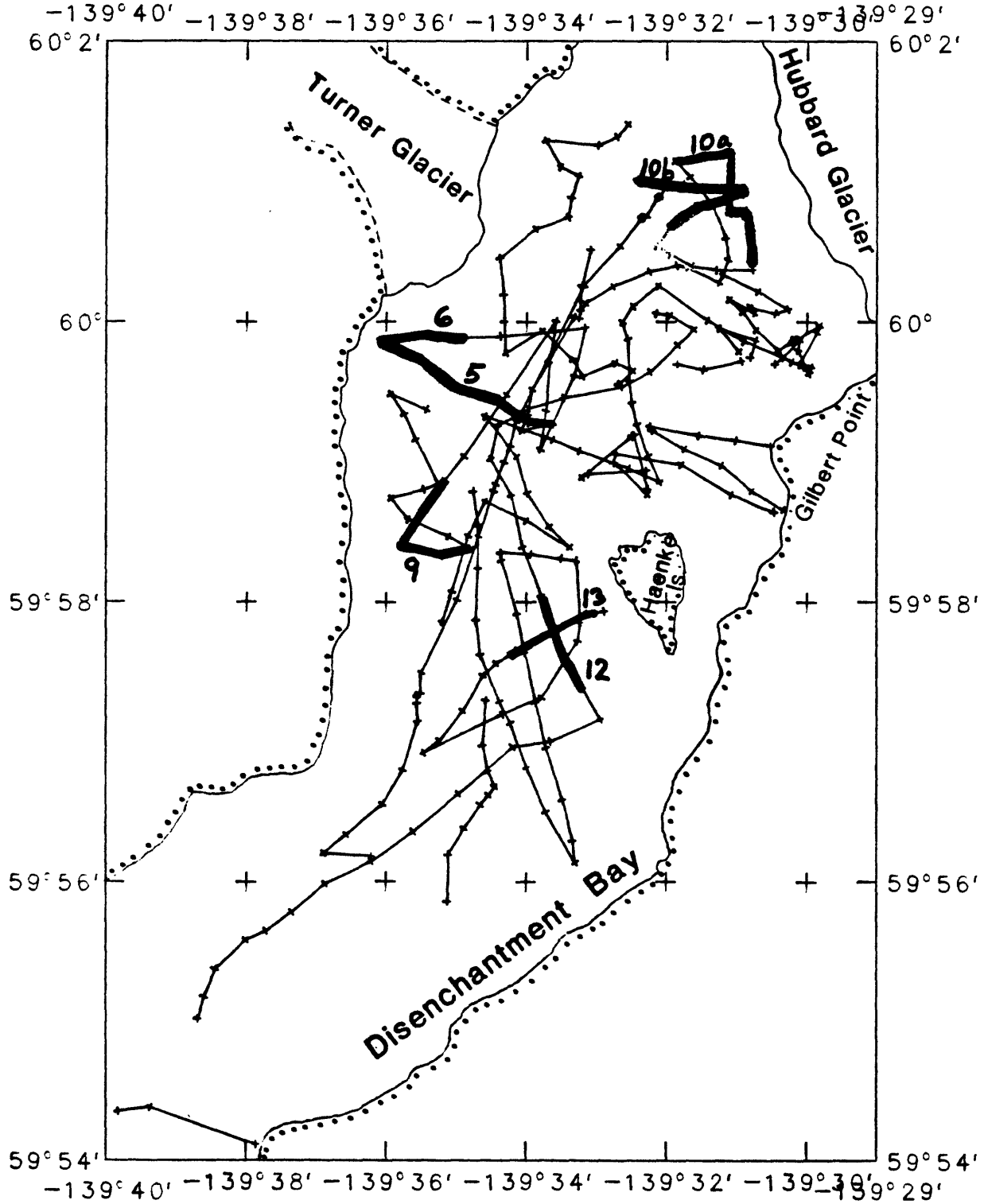

Figure 2a. Trackline map showing high-resolution seismic-reflection coverage in Disenchantment Bay. Numbered thicker lines locate illustrated profiles. See figure 1 for location.

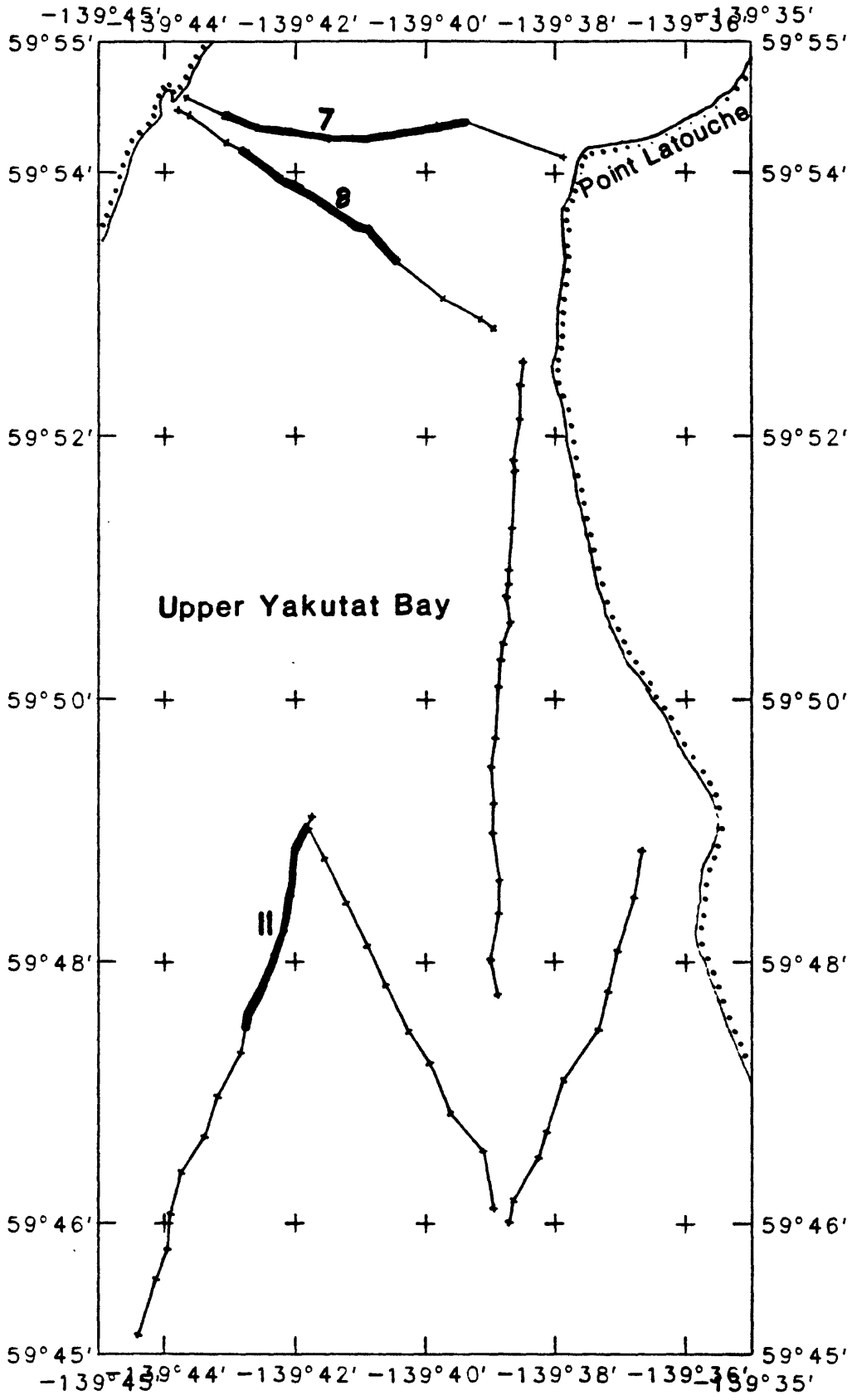

Figure 2b. High-resolution seismic-reflection profile lines in upper Yakutat Bay. Numbered thicker lines locate illustrated profiles. See figure 1 for general location in greater Yakutat Bay.

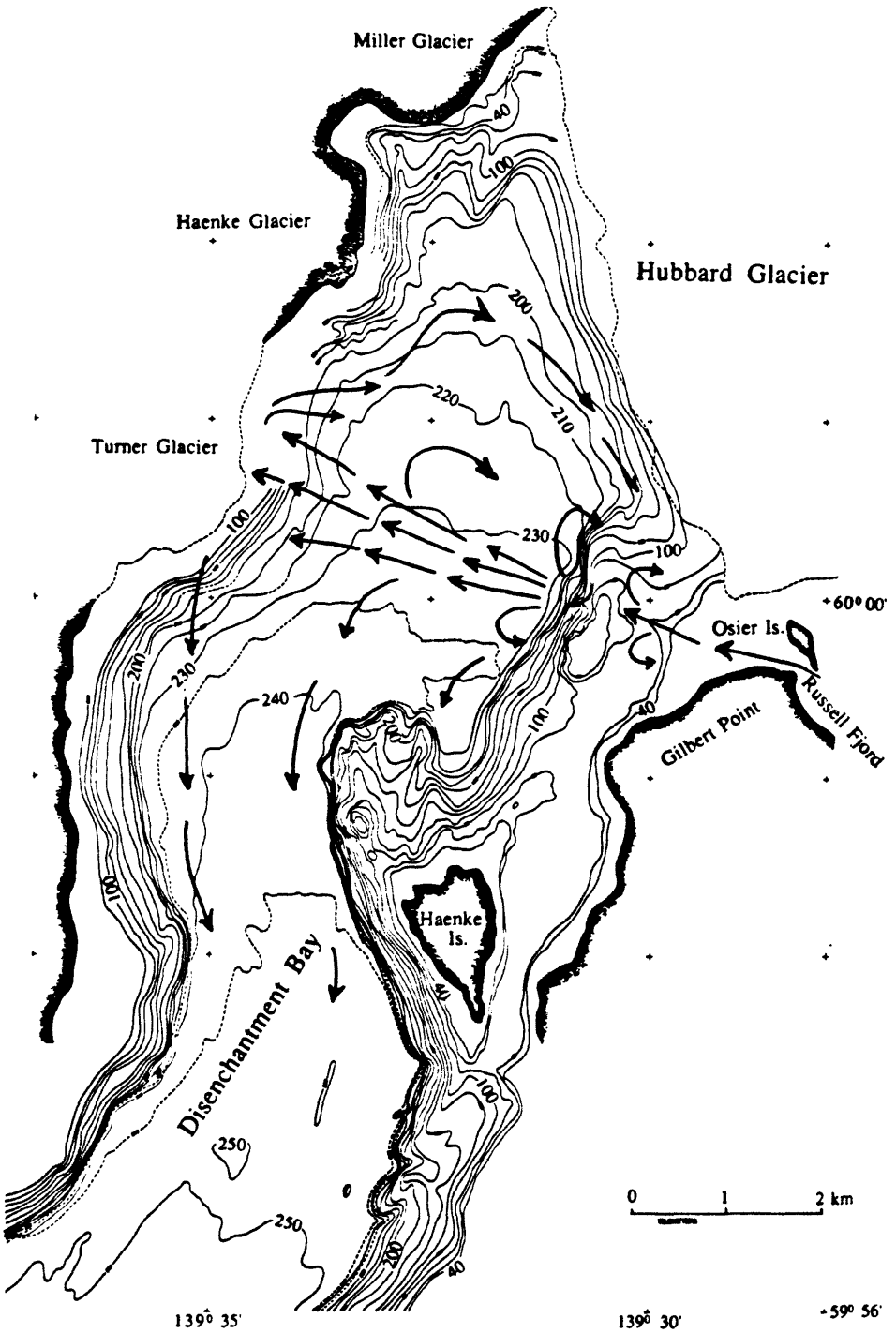

Figure 3. Detailed bathymetry of Disenchantment Bay. Contoured from NOAA depth soundings (Hydrographic Surveys 9778 & 9779) collected in 1978. Contour intervals are 20 m on the fjord walls and 10 m on deep basin floor, supplemented by 5 m intervals at >230 m depth. Location of ice face of Hubbard Glacier approximated from July 20, 1990 aerial photographs furnished by Robert Krimmel, USGS, Tacoma, Washington. Arrows show generalized path of outburst flood waters (October 8, 1986) based on descriptions by Mayo (written memorandum, November 19, 1986; 1989).

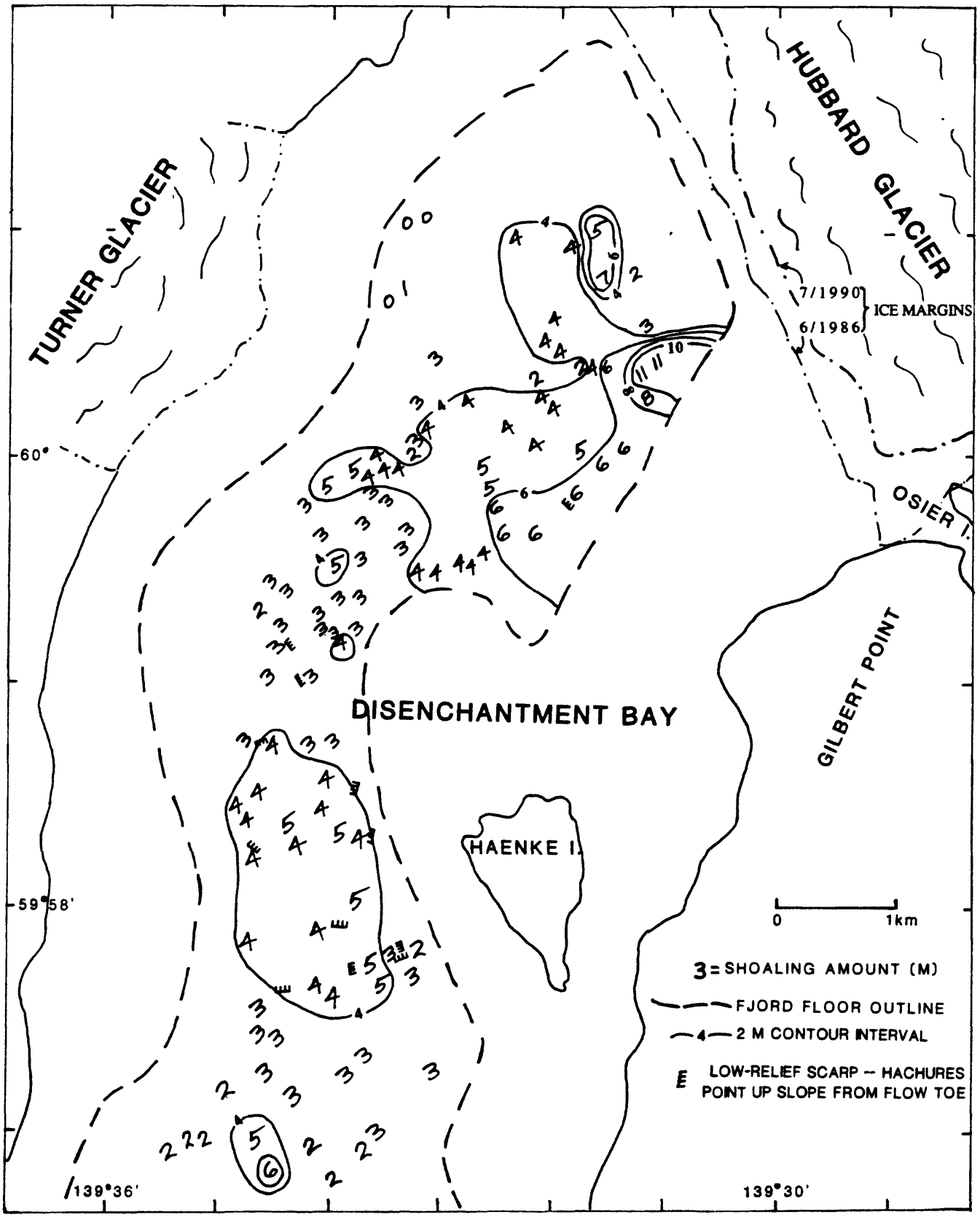

Figure 4. Map of deep fjord basin floor in Disenchantment Bay showing amount of shoaling that has occurred between 1978 (see contoured bathymetry Fig. 3) and 1991 (cruise K1-91). Also included are locations of low-relief scarps mapped from high-resolution seismic-reflection profiles. Ice margin positions: June, 1986 (Mayo, 1989); July, 1990 (aerial photo--see Fig. 3).

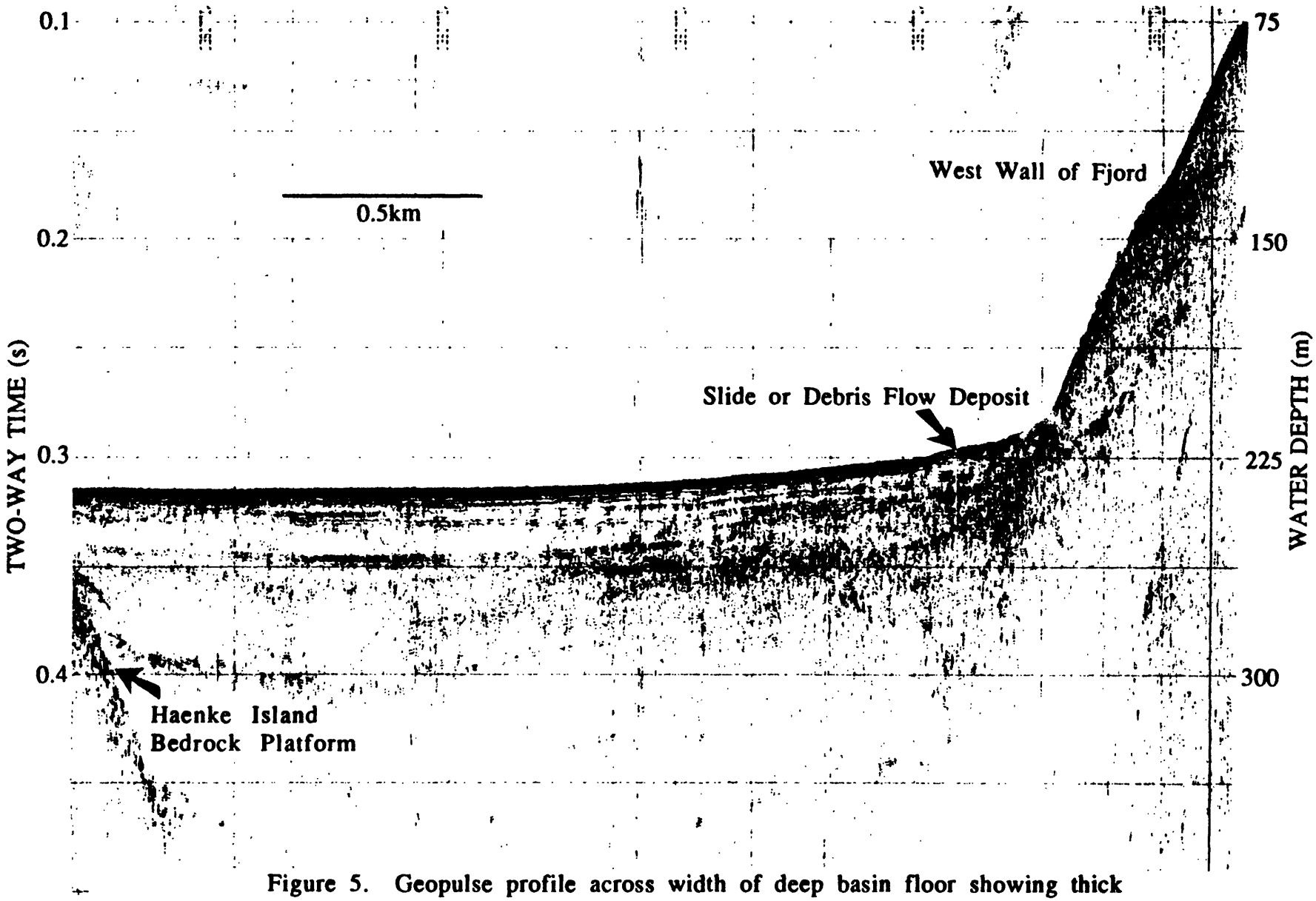

Figure 5. Geopulse profile across width of deep basin floor showing thick (>150 m) sequence of sediment. Note slide or debris flow deposit at base of west wall; disrupted, discontinuous reflections at depth in sediment (>25 m) in west half of basin also are indicative of a mass movement deposit. See figure 2a for location. Vertical exaggeration (V.E.)~7x

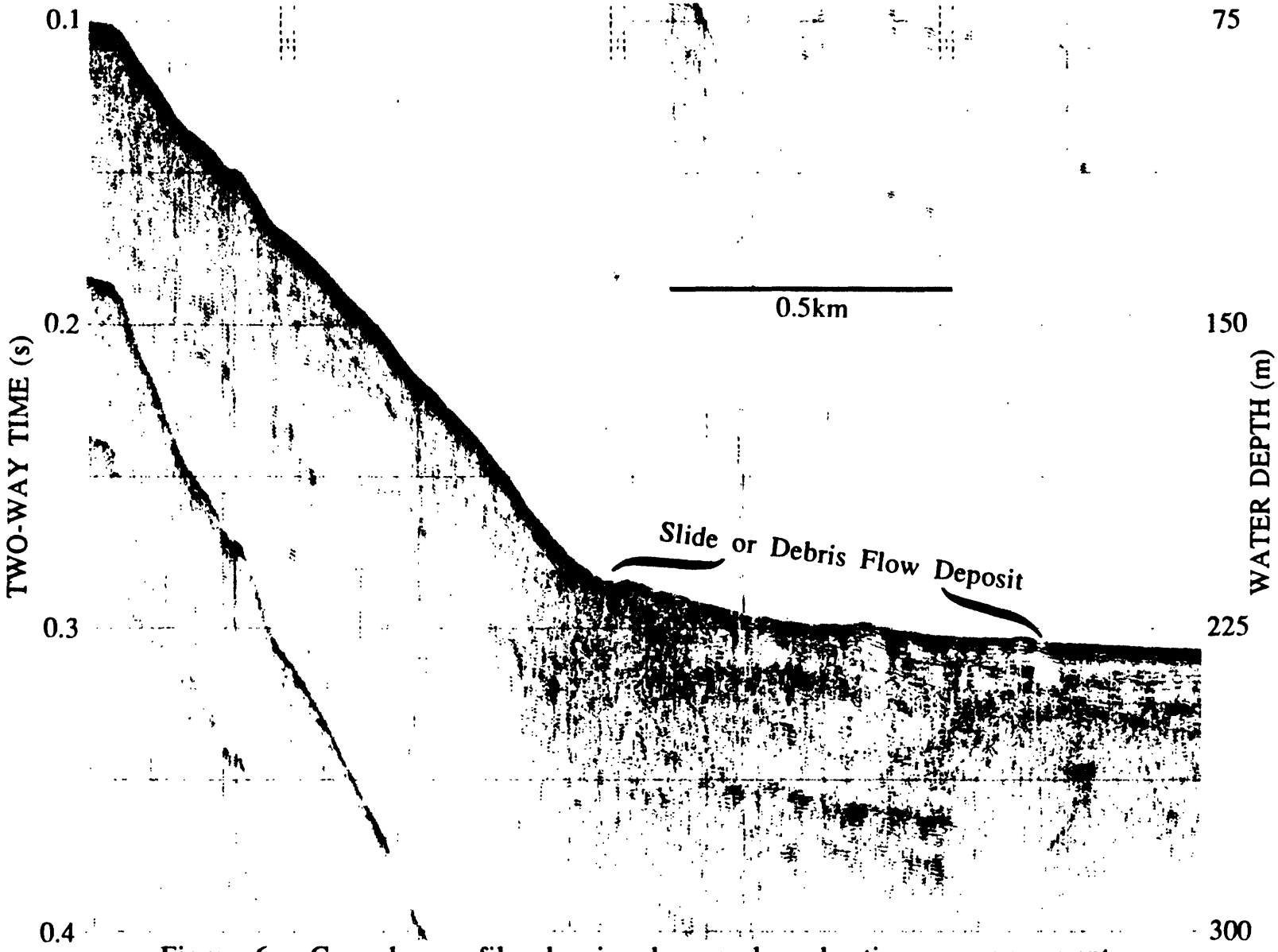

Figure 6. Geopulse profile showing hummocky, chaotic mass movement debris reflections at base of west wall near Turner Glacier. This profile is just north of profile shown in figure 5, illustrating abundance of mass movement deposits that contribute to fjord fill. See figure 2a for location. V.E.~7x

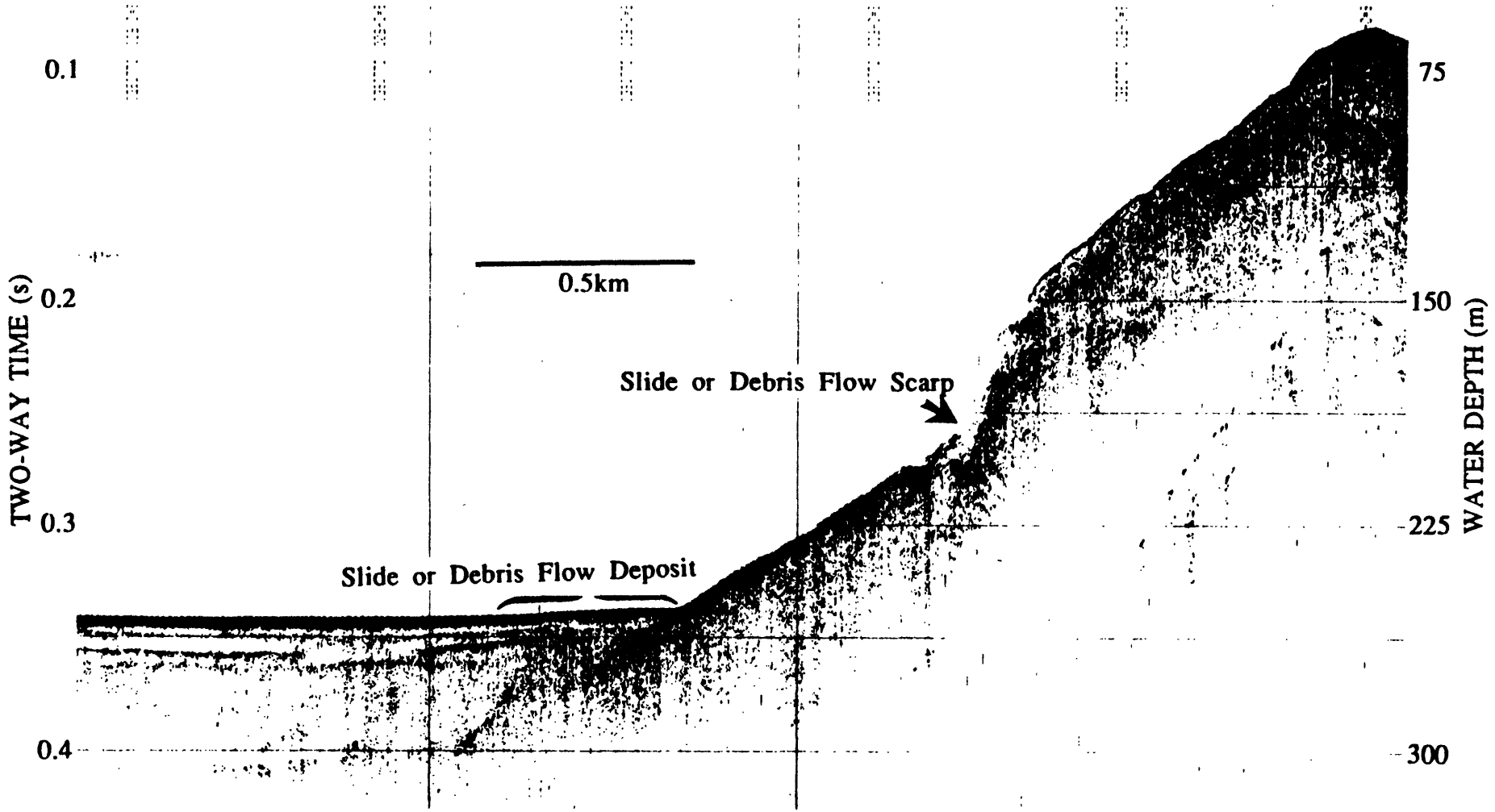

Figure 7. Geopulse profile illustrating 50 m high scarp on west wall of upper Yakutat Bay and accumulation of mass movement debris at base of slope. See figure 2b for location. V.E~7x.

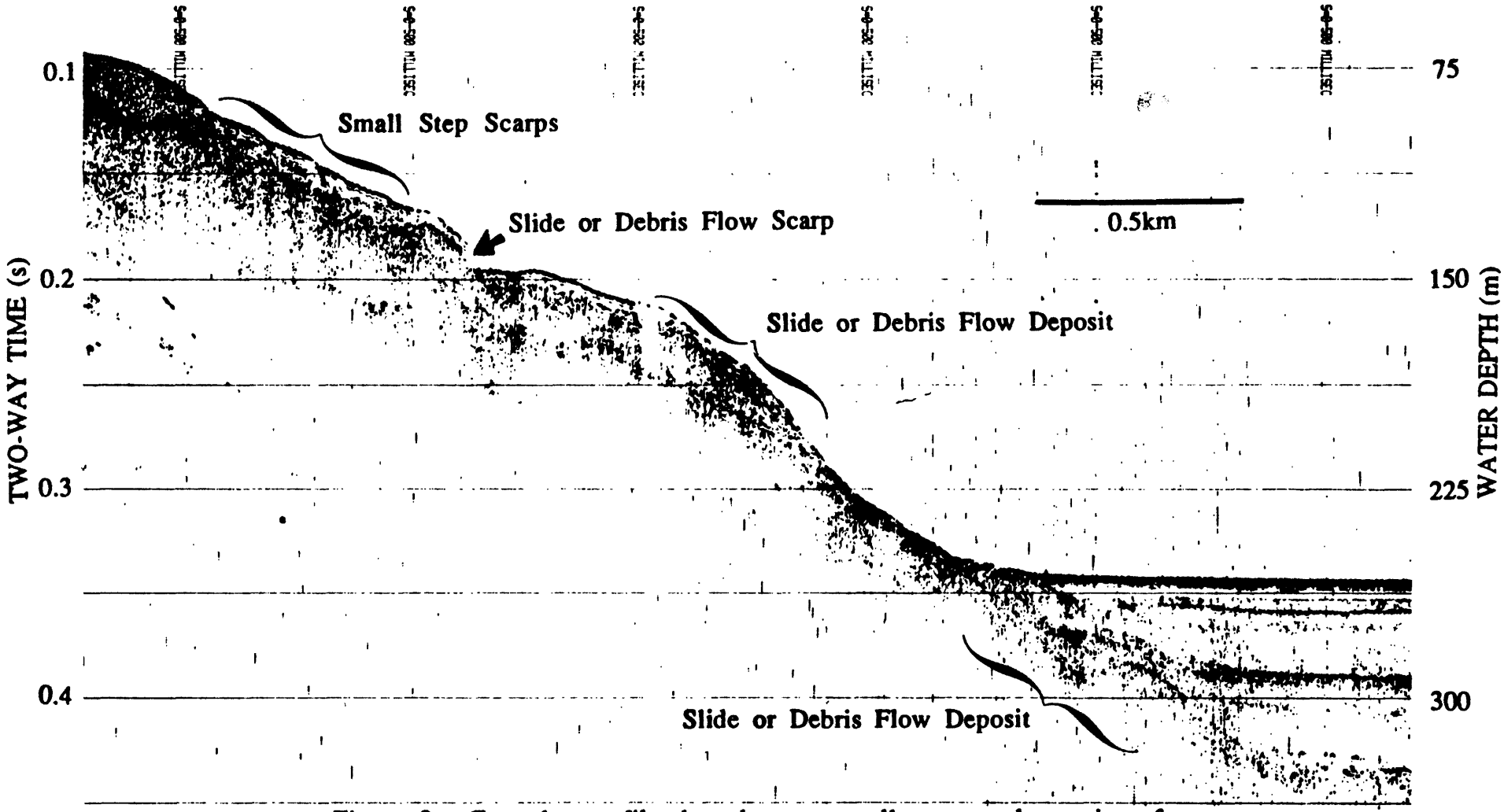

Figure 8. Geopulse profile that shows a small scarp and a series of small step scarps on west wall of the fjord and an accumulation of mass movement debris in basin at base of wall. See figure 2b for location. V.E.~7x.

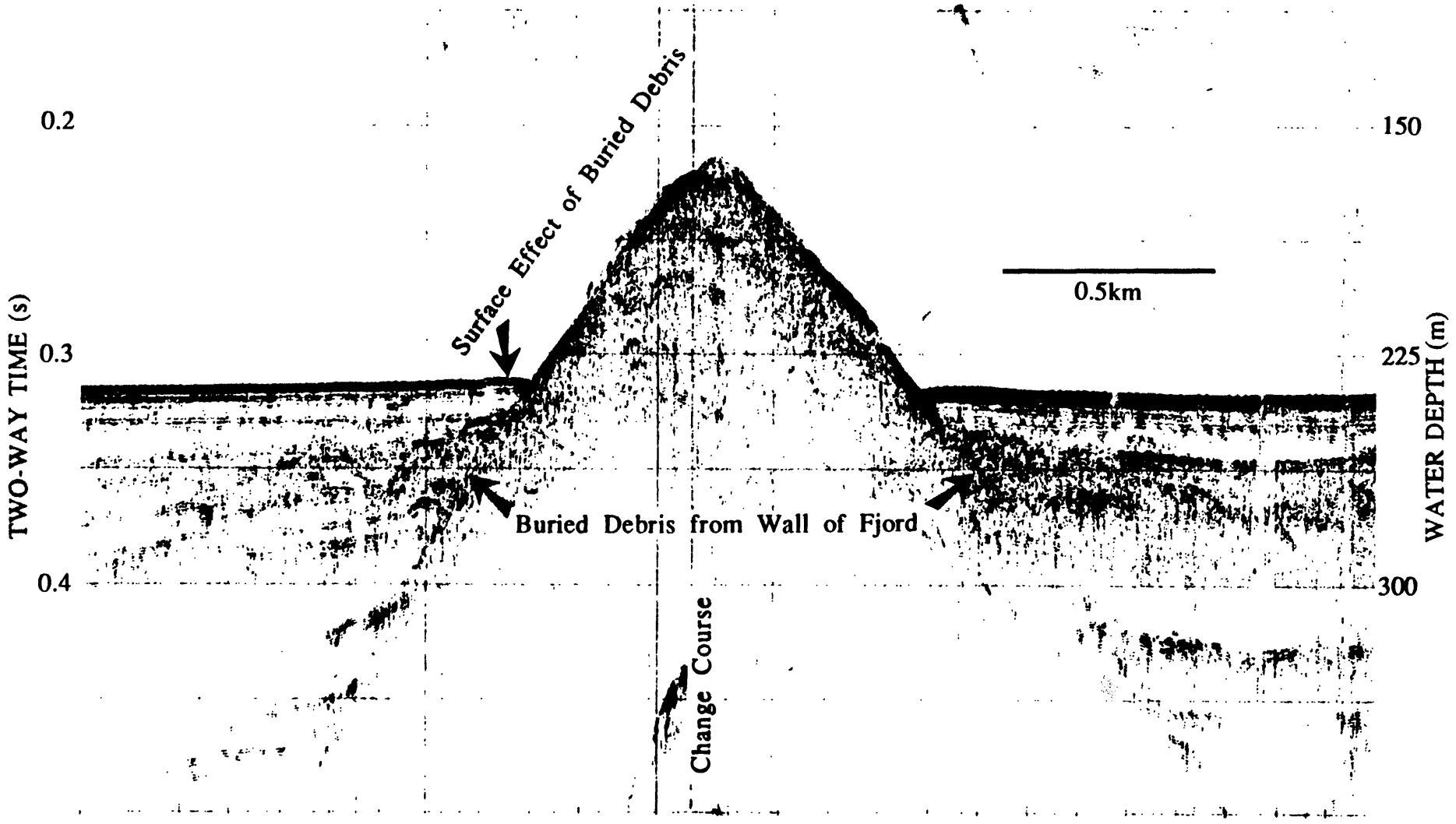

Figure 9. The west side of two adjacent Geopulse profiles shows a buried mass movement deposit at the base of the fjord wall near Turner Glacier. See figure 2a for location. V.E.~7x.

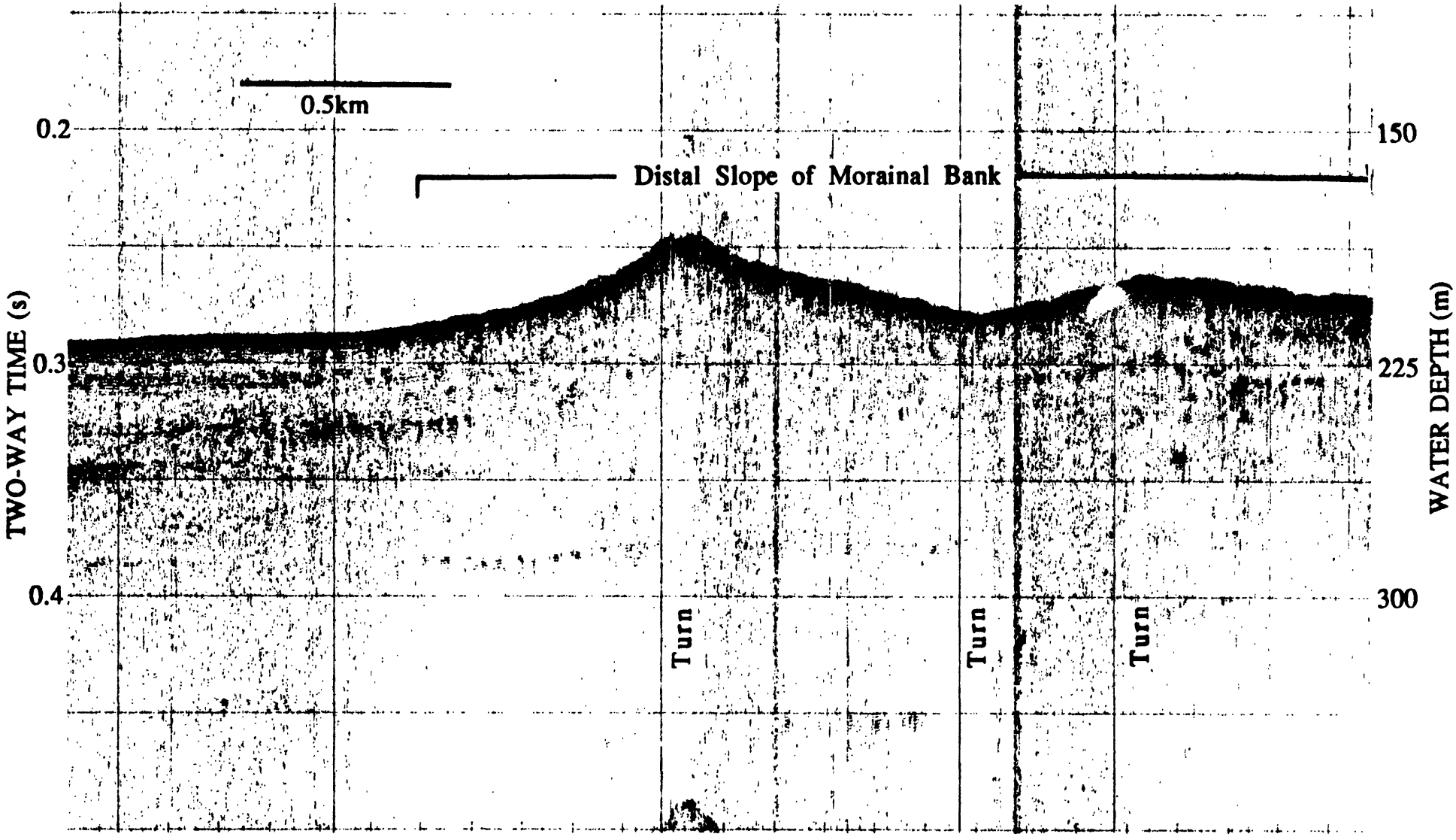

Figure 10a. Three parts of saw-tooth segment of acoustic profile line that show seismic-reflection character of distal part of morainal bank that forms pinning point of Hubbard Glacier. See figure 2a for location. V.E.~7x.

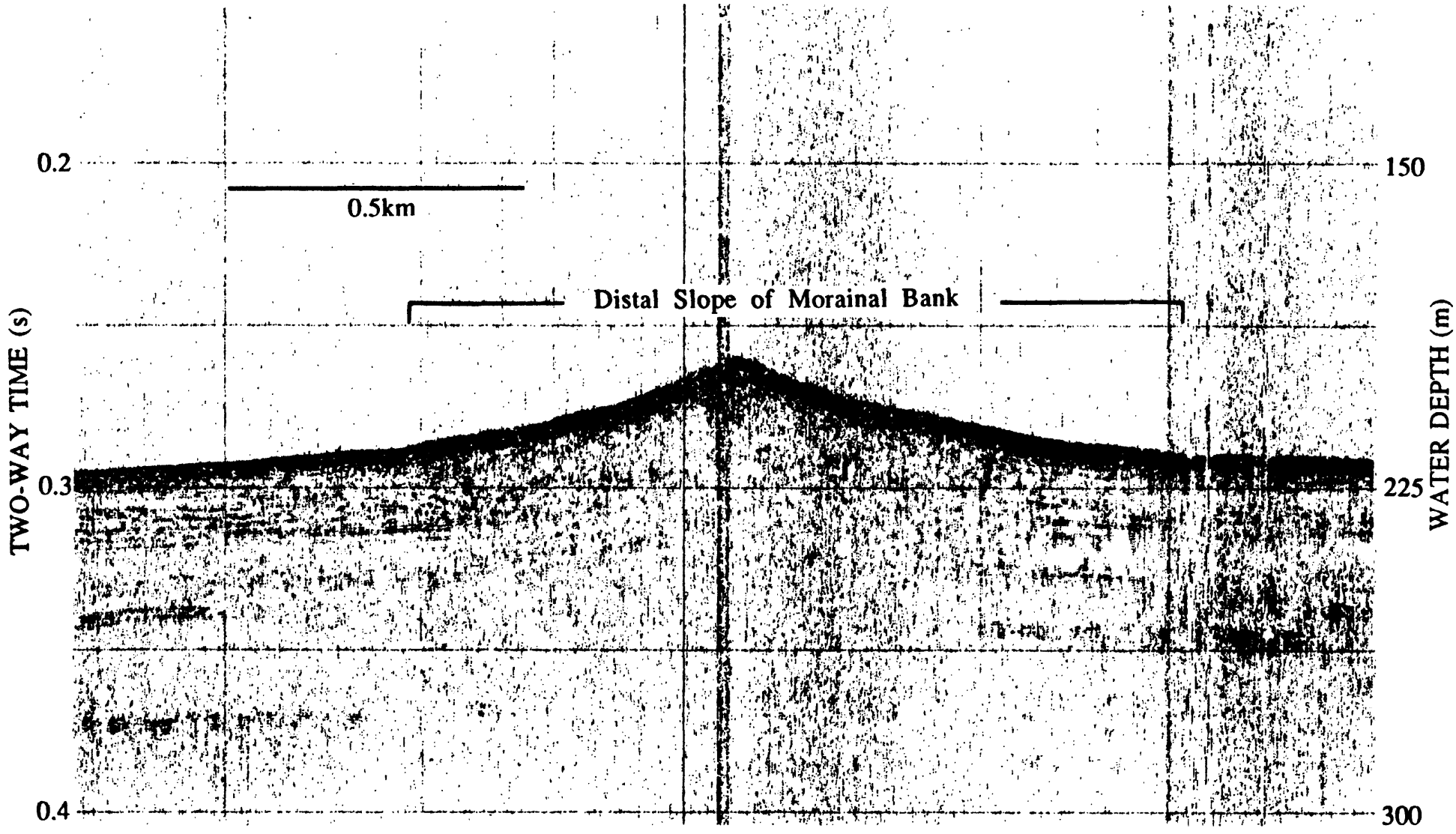

Figure 10b. Geopulse profile of distal morainal bank. Change of course (c/c) at center of profile is about 0.5 km from Hubbard Glacier ice face. See figure 2a for location. V.E.~7x.

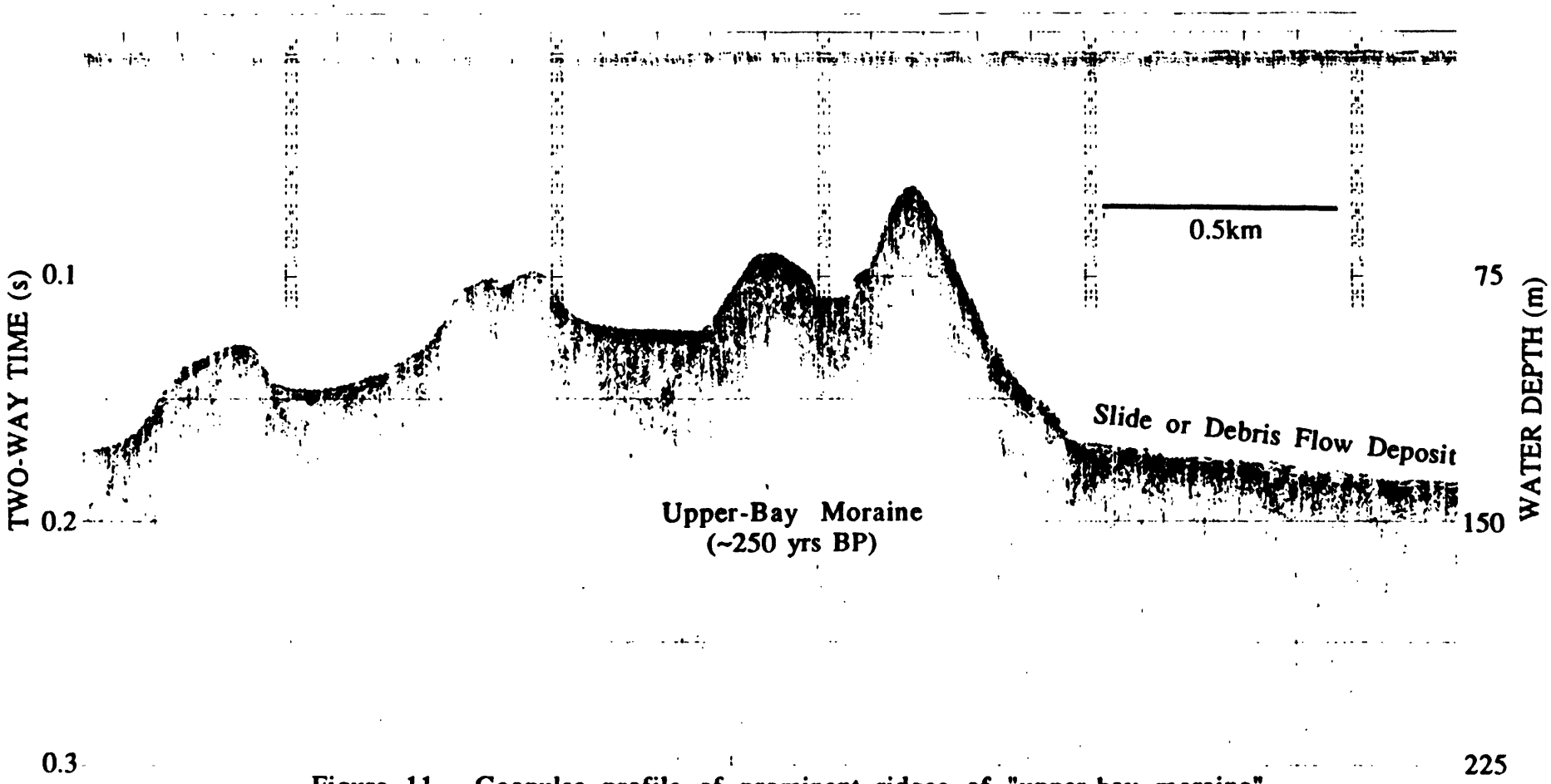

Figure 11. Geopulse profile of prominent ridges of "upper-bay moraine" of upper Yakutat Bay showing hummocky slide or debris flow surface off south flank. Note sediment accumulation in small intra-morainal depressions. See figure 2b for location. V.E.~7x.

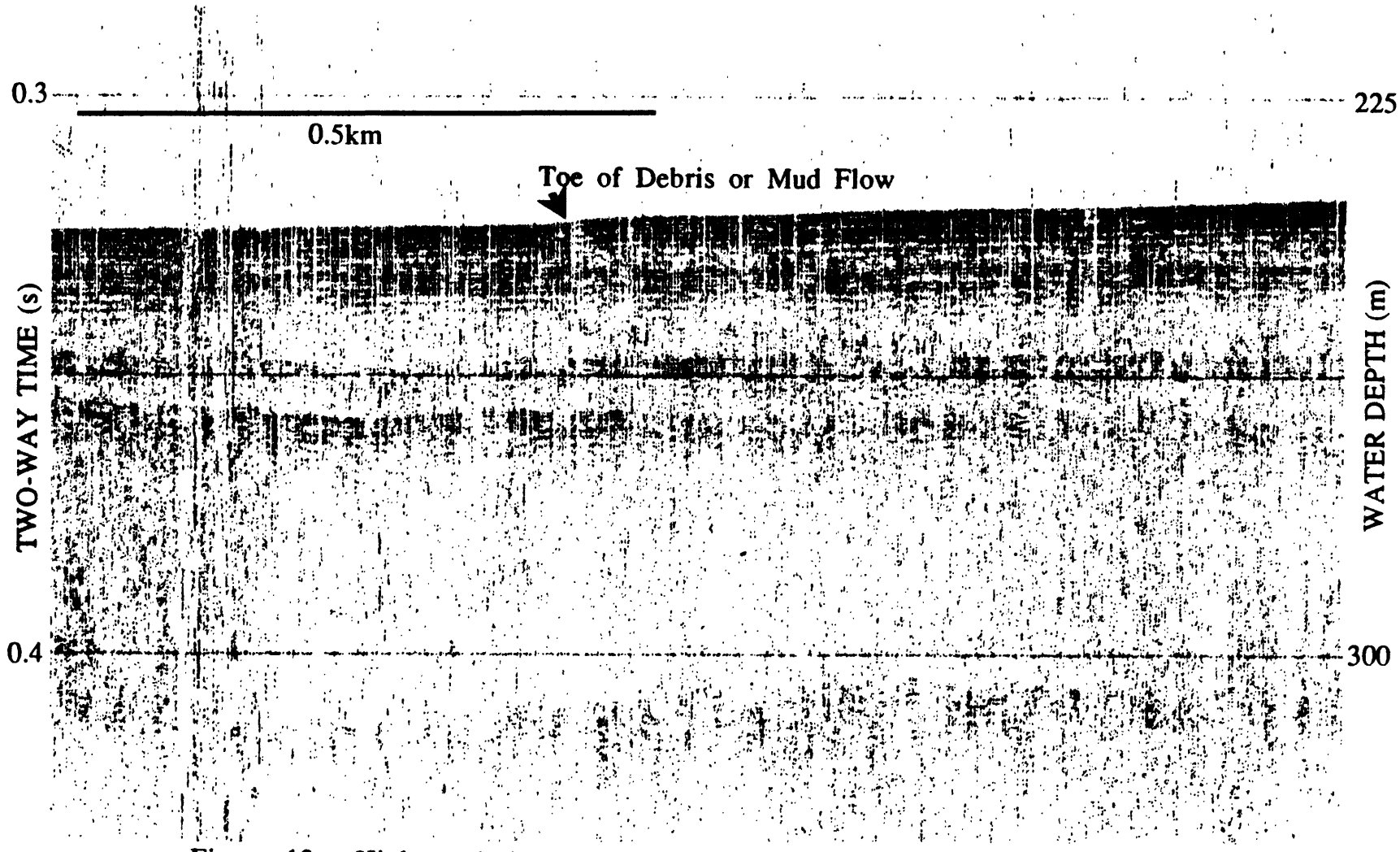

Figure 12. High-resolution Geopulse profile of deep fjord floor west-southwest of Haenke Island showing subtle scarp of debris or mud flow. See figure 2a for location. V.E.~7x.

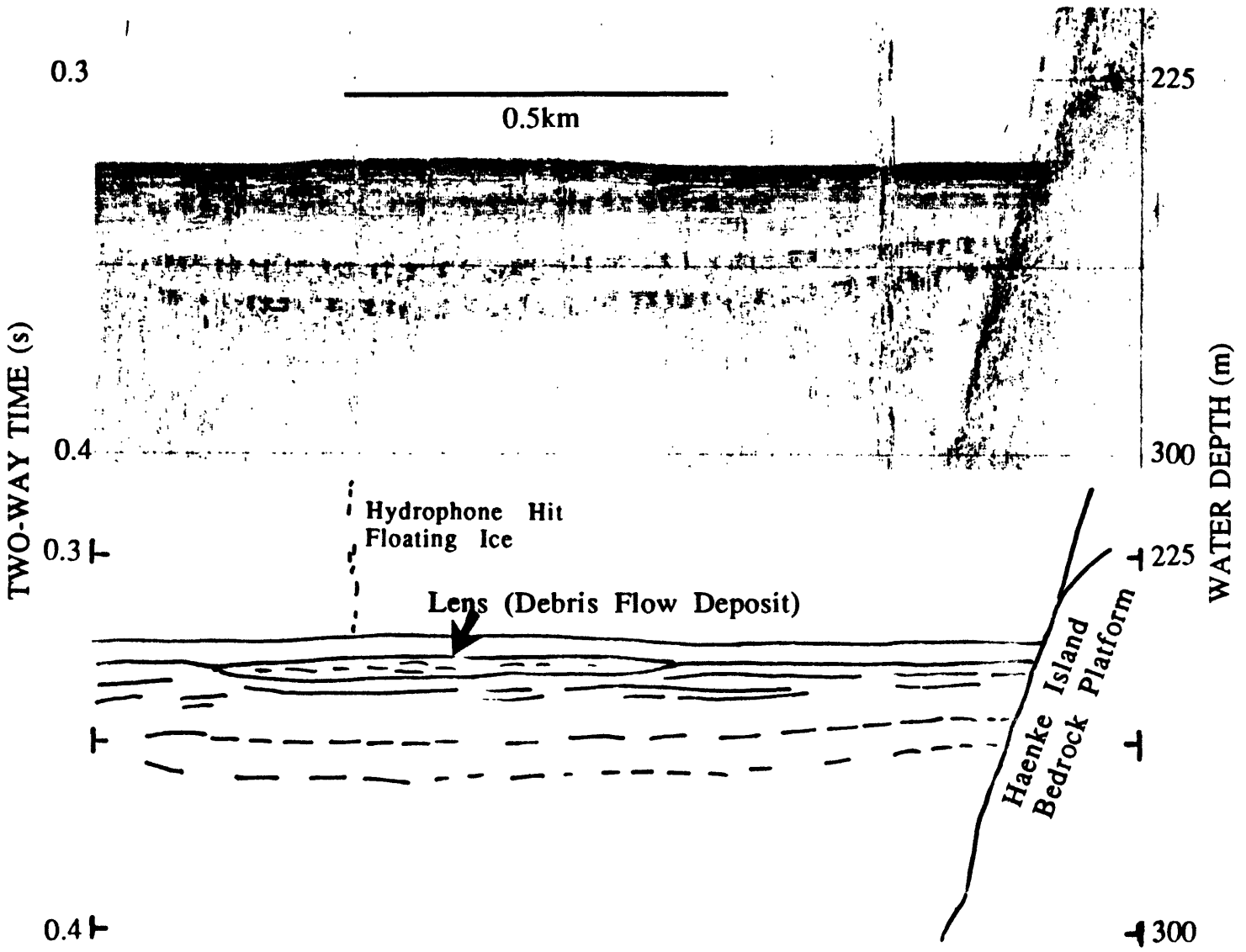

Figure 13. High-resolution Geopulse profile showing buried lens-shaped flow deposit within deep fjord floor sediment fill. See figure 2a for location. V.E.~7x.

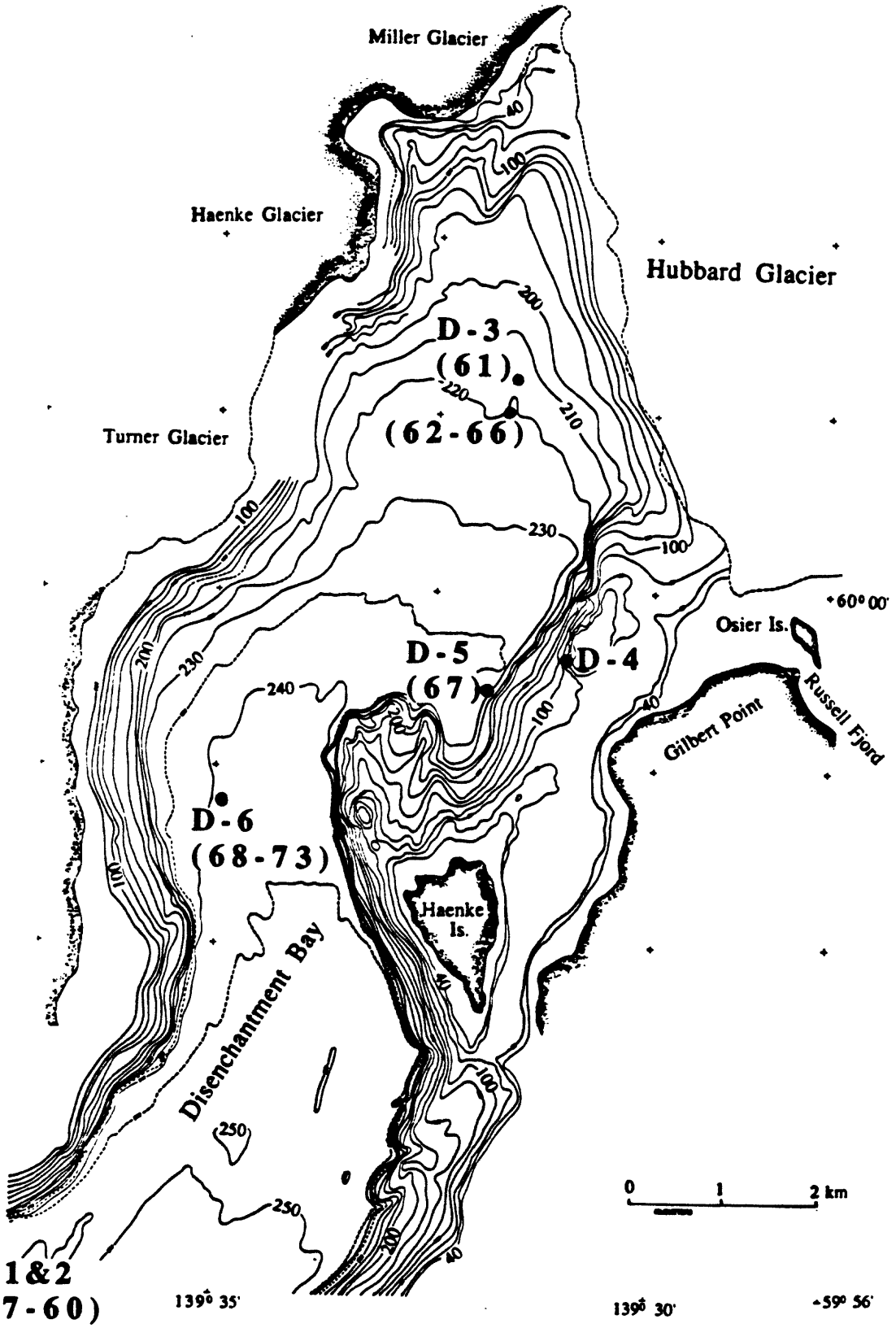

Figure 14. Location map of ROV dive sites D-1 through D-6 and water column samples (57-73).

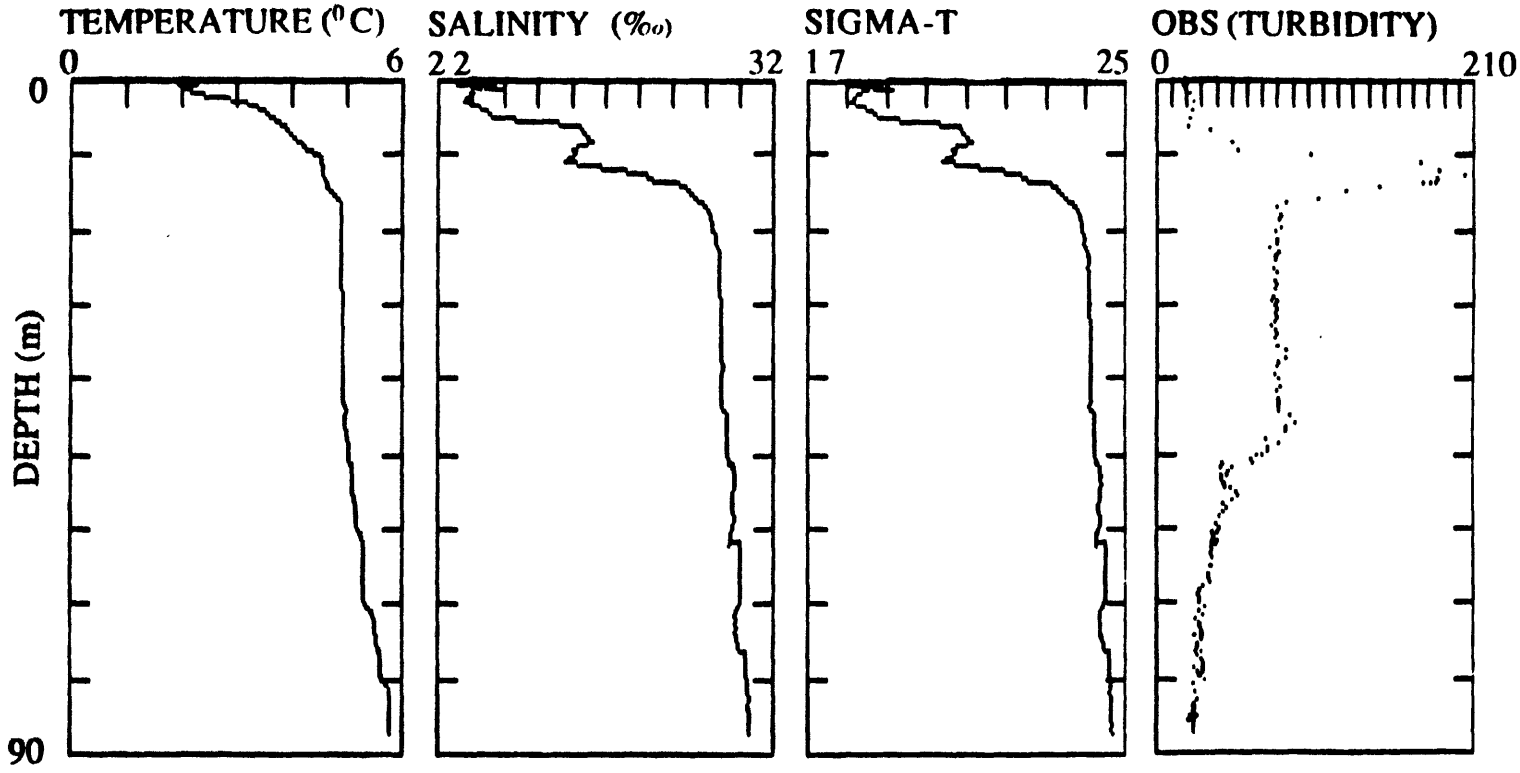

Figure 15. Profiles of temperature, salinity, sigma-t, and OBS collected from dive site 1 on June 24, 1991. Dive began at 0905 hours (Alaska day light time) and ended short of the bottom. (Local time throughout). See figure 14 for locations of all dive sites.

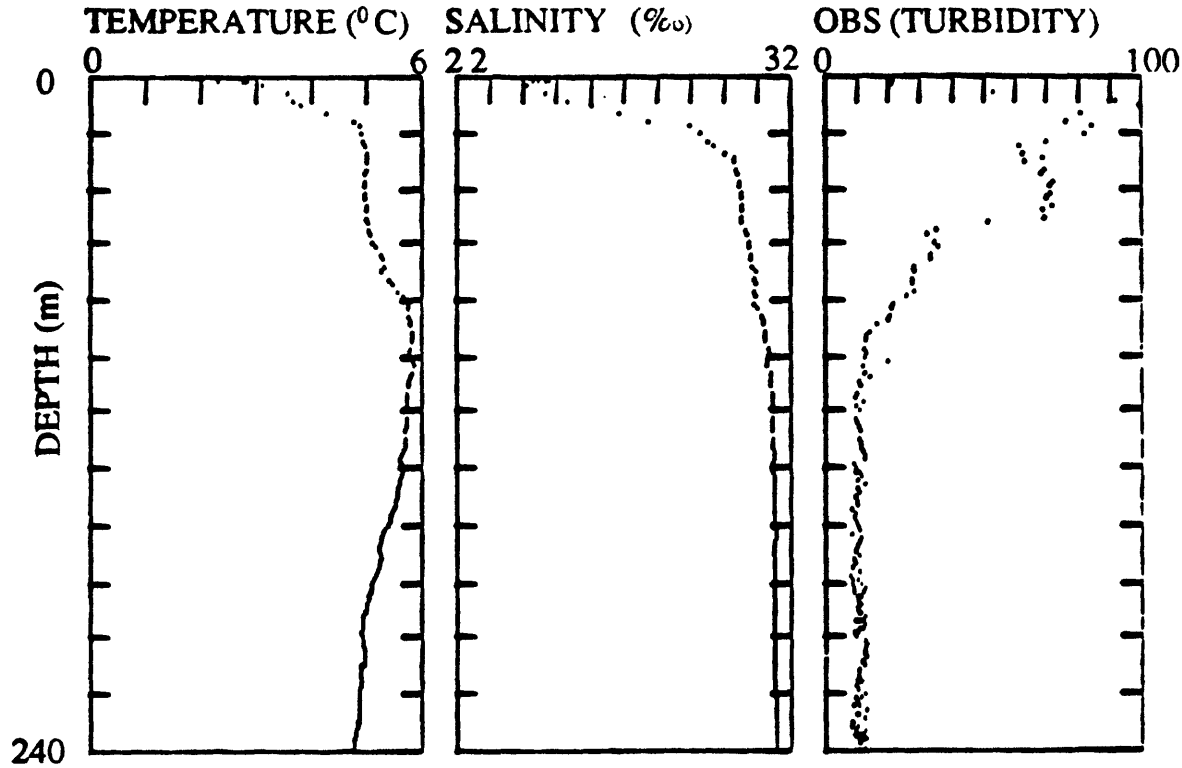

Figure 16a. Profiles of temperature, salinity, and OBS collected from dive site 2 on June 24, 1991. Descent began at 1016 hours.

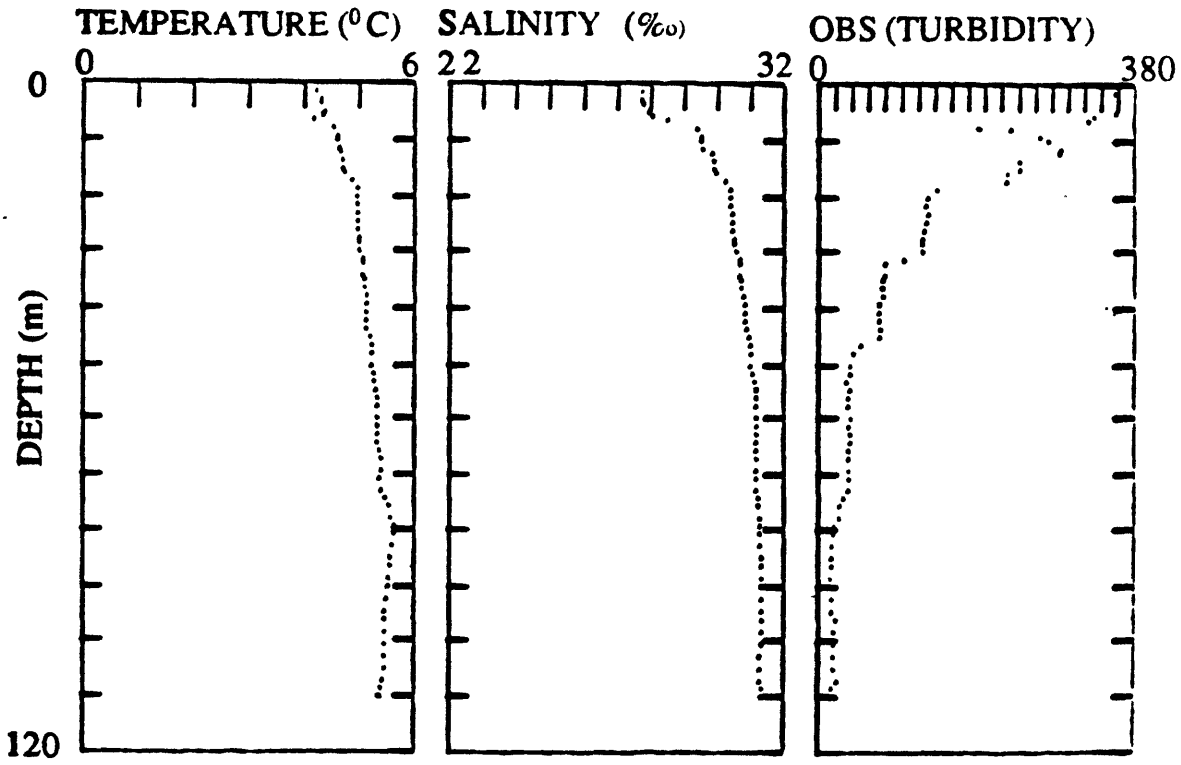

Figure 16b. Profiles of temperature, salinity, and OBS collected from dive site 3 on June 24, 1991. ROV descent was located approximately 50 m away from Hubbard ice face and began at 1445 hours. Dive did not reach bottom.

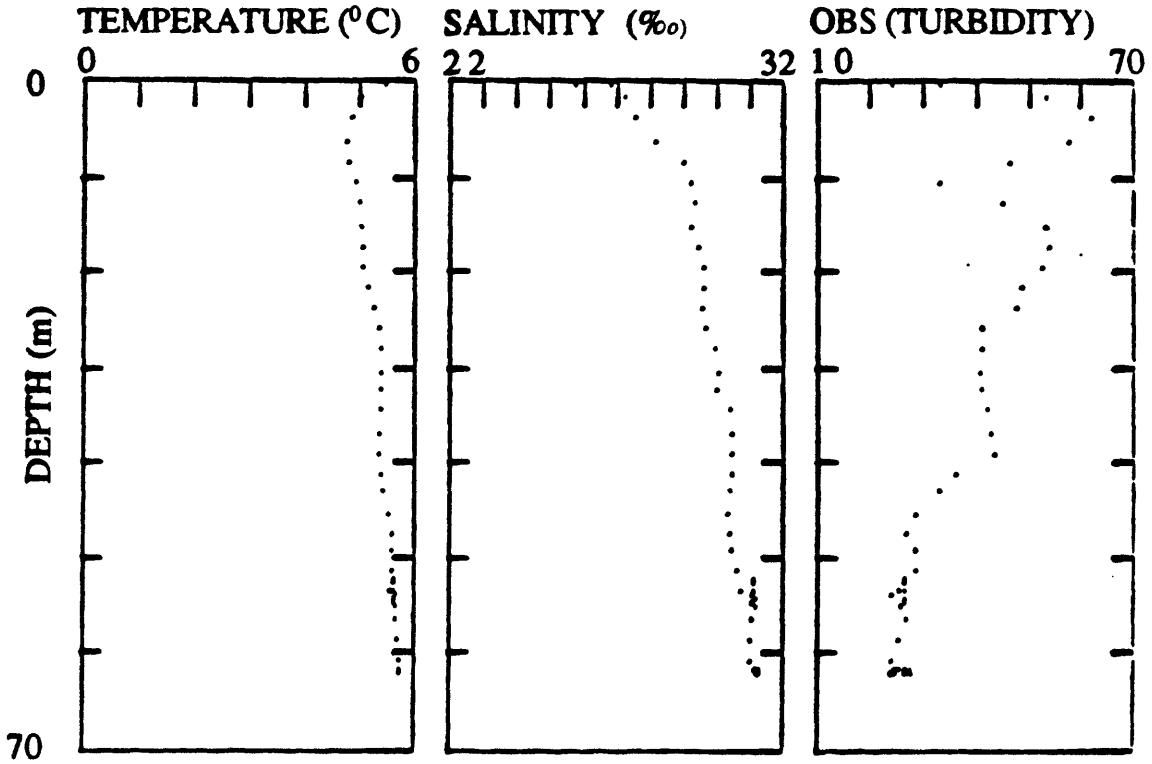

Figure 17a. Profiles of temperature, salinity, and OBS collected during descent at dive site 4 on June 27, 1991, adjacent to Russell Fjord breakout site. Descent began at 1049 hours, during ebb tide.

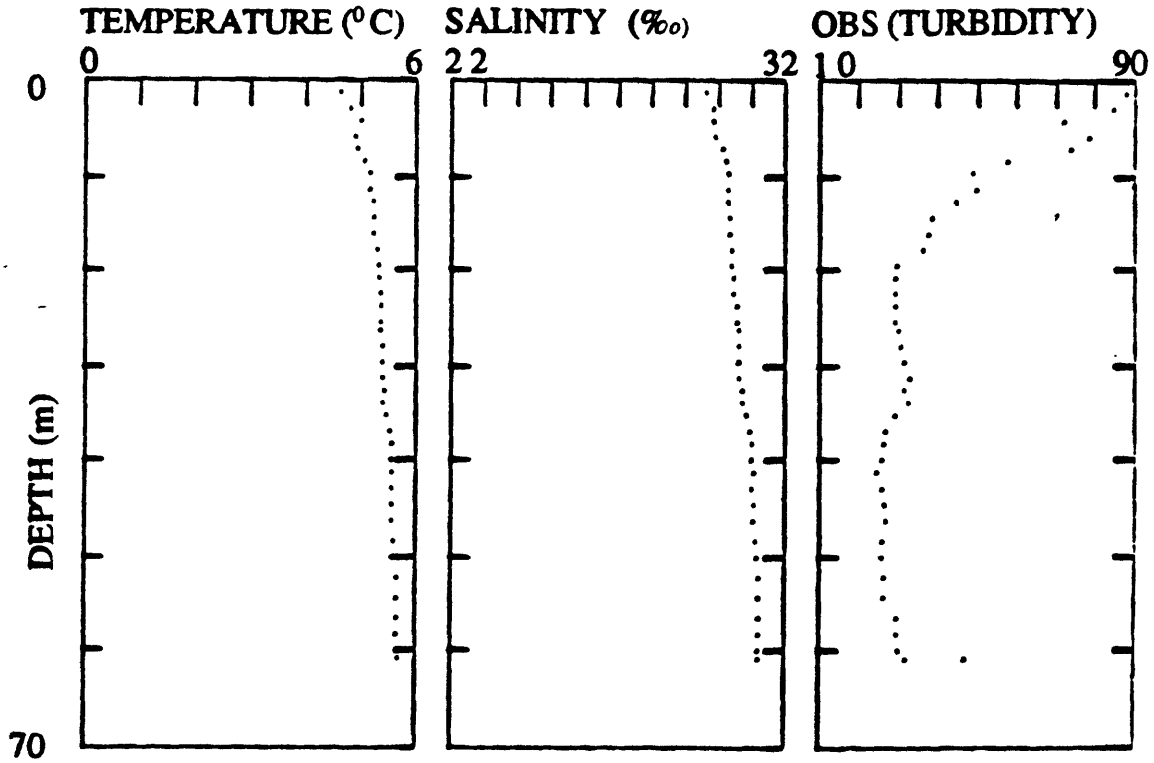

Figure 17b. Profiles of temperature, salinity, and OBS turbidity collected from dive site 4 on June 27, 1991, adjacent to Russell Fjord breakout site. This profile was collected during ascent from fjord floor at 1111 hours.

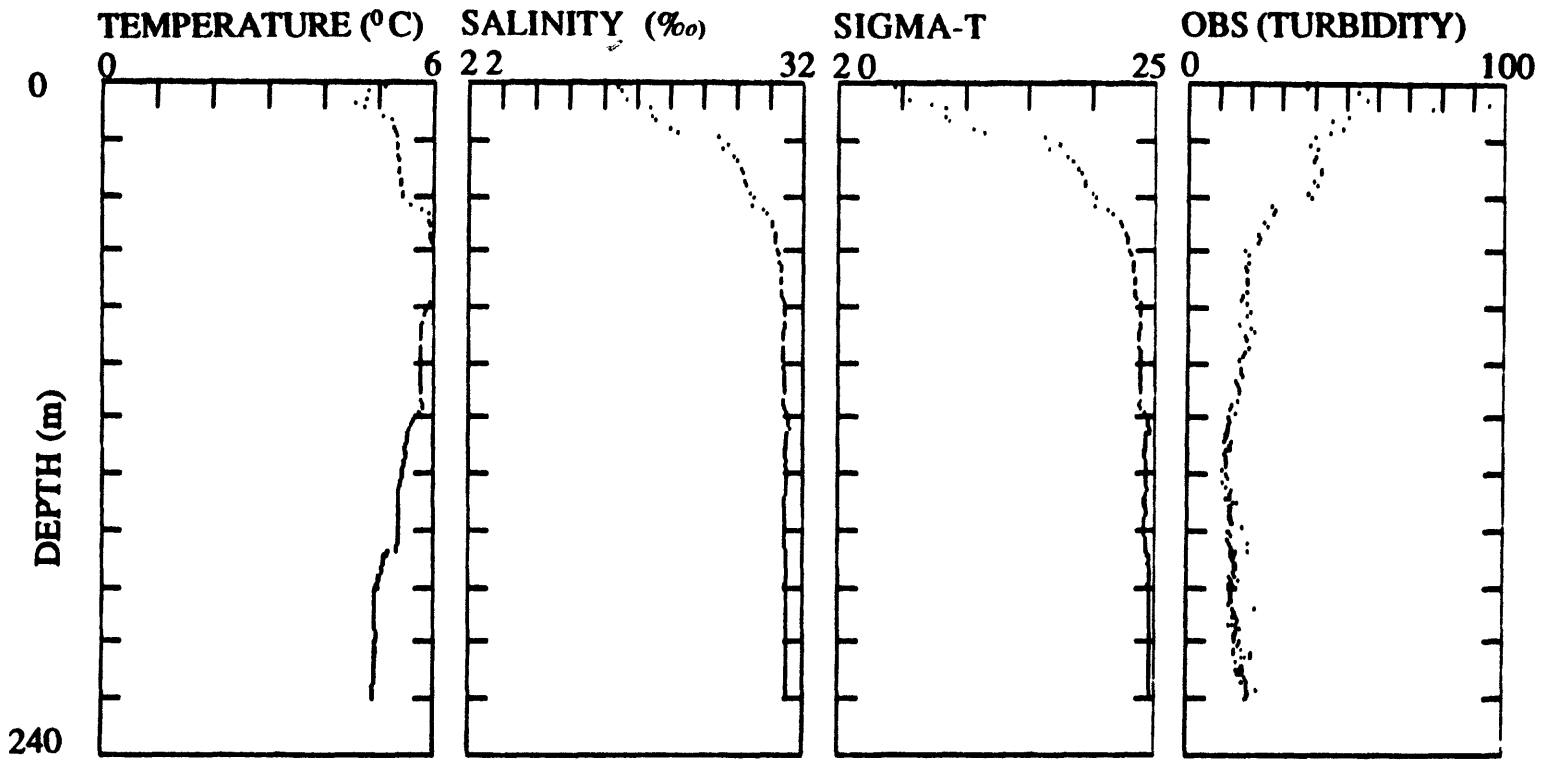

Figure 18. Profiles of temperature, salinity, sigma-t, and OBS turbidity collected from dive site 5 on June 27, 1991. The dive began at 1257 hours and reached bottom at 1322 hours.

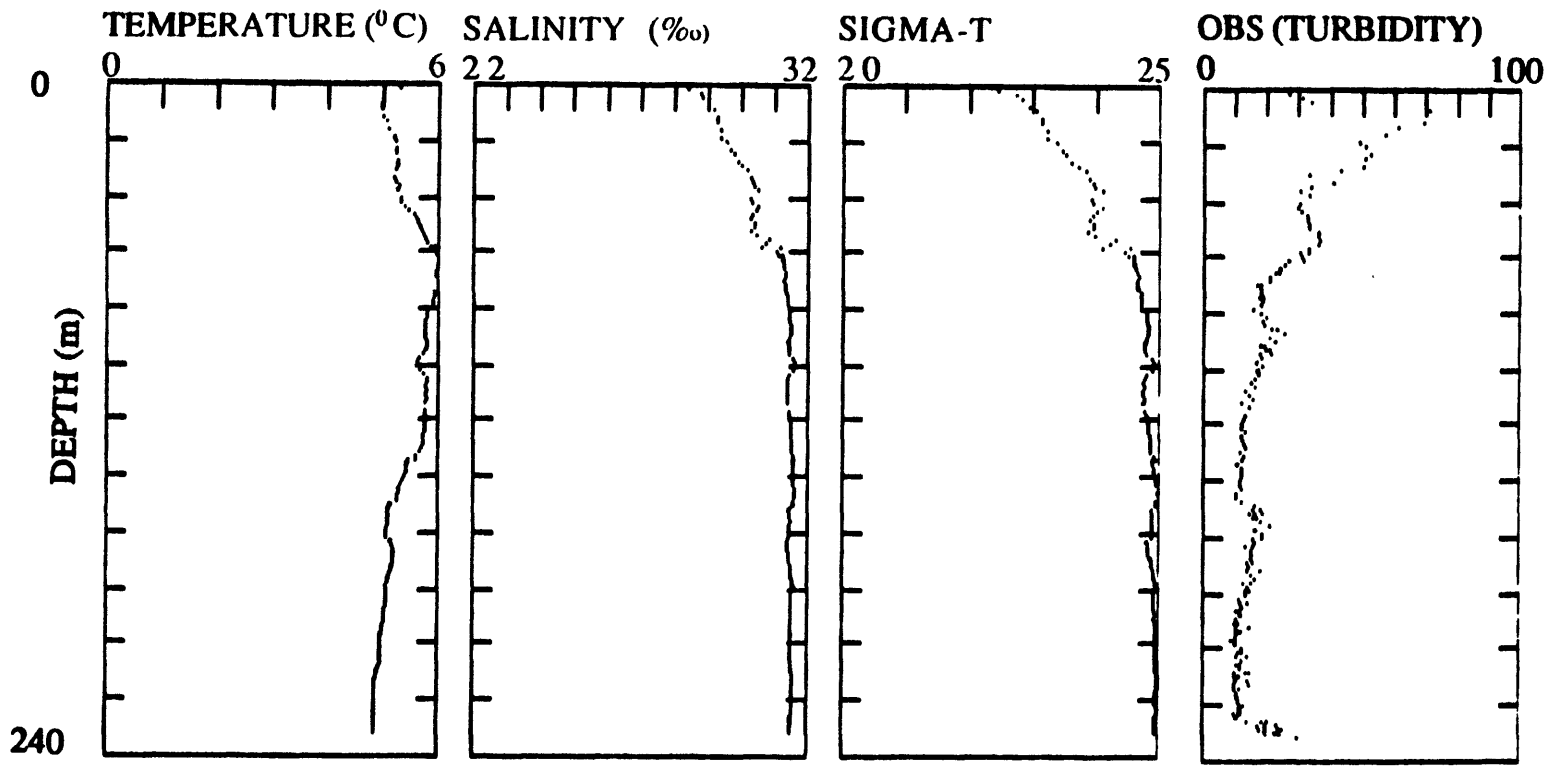

Figure 19a. Profiles of temperature, salinity, sigma-t, and OBS collected from dive site 6 on June 27, 1991. Dive began at 1447 hours and reached bottom at 1507 hours.

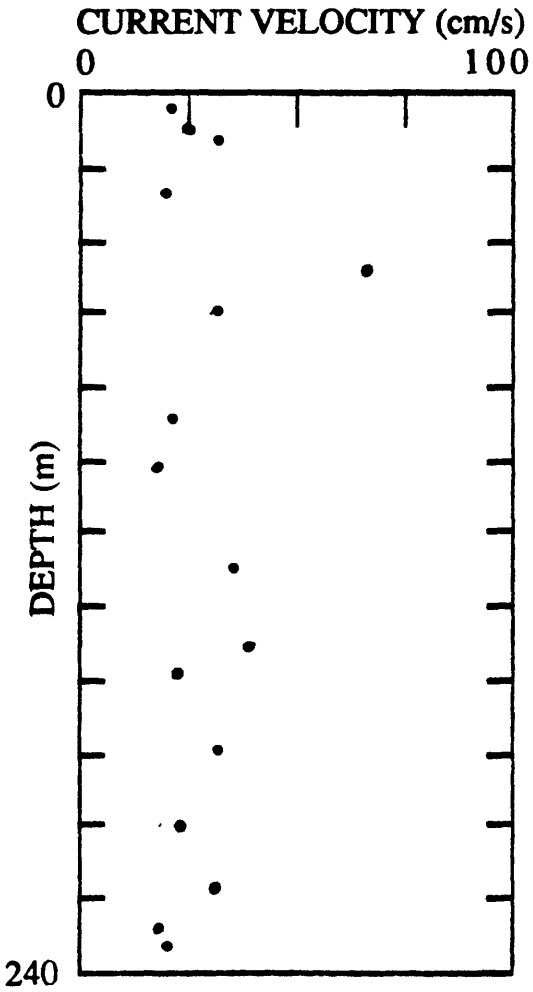

Figure 19b. Current speed measured on ascent at dive site 6. Data are mean values of 20 to 24 readings at each depth. Current velocity at 40 m depth could not be measured because ROV was constantly spinning on its tether. Speed exceeded other depths, but magnitude is unknown.

Table 1. Water Samples Collected from Disenchantment Bay *RV KARLUK* Cruise K1-91-YB (See Fig. 14 for locations).

DATE	TIME	DEPTH (m)	CONCENTRATION (mg/L)	LOCATION	SAMPLE NUMBER
6-24-91	1057	30	159	Dive 2	HG91-57
6-24-91	1102	20	182	Dive 2	HG91-58
6-24-91	1106	10	196	Dive 2	HG91-59
6-24-91	1110	5	155	Dive 2	HG91-60
6-24-91	1434	0	602	Dive 3	HG91-61
6-24-91	1545	11	530	Dive 3	HG91-63
6-24-91	1550	20	337	Dive 3	HG91-64
6-24-91	1602	36	270	Dive 3	HG91-66
6-24-91	1619	5	63	Dive 3	HG91-62
6-27-91	1354	0	85	Dive 5	HG91-67
6-27-91	1607	0	19	Dive 6	HG91-68
6-27-91	1628	23	89	Dive 6	HG91-69
6-27-91	1635	17	78	Dive 6	HG91-70
6-27-91	1640	10	67	Dive 6	HG91-71
6-27-91	1642	5	62	Dive 6	HG91-72
6-27-91	1648	35	67	Dive 6	HG91-73